Helicobacter-mediated gastric cancer development and progression through YAP/TAZ signal regulation

Yu, Byeong Min

Department of Medicine
Graduate School
Yonsei University

Helicobacter-mediated gastric cancer development and progression through YAP/TAZ signal regulation

Advisor : Lee, Yong Chan

A Dissertation Submitted
to the Department of Medicine
and the Committee on Graduate School
of Yonsei University in Partial Fulfillment of the
Requirements for the Degree of
Doctor of Philosophy in Medicine

Yu, Byeong Min

June 2025

Helicobacter-mediated gastric cancer development and progression through YAP/TAZ signal regulation

This certifies that the Dissertation of Yu, Byeong Min is approved

Thesis Supervisor [Lee, Yong Chan]

Thesis Committee Member [Nam, Ki Teak]

Thesis Committee Member [Kim, Ji Hyun]

Thesis Committee Member [Kim, Hye Young]

Thesis Committee Member [Youn,Young Hoon]

Department of Medicine
Graduate School
Yonsei University
December 2024

ACKNOWLEDGEMENTS

I would like to begin by expressing my sincerest gratitude to Professor Yong Chan Lee of Yonsei University, who provided invaluable guidance and support throughout my master's and doctoral studies, influencing my research trajectory in significant ways. Furthermore, I would like to express my gratitude to the members of my doctoral examination committee: I would like to express my gratitude to Professors Ki Teak Nam, Ji Hyun Kim, Hye Young Kim and Young Hoon Yoon I am truly grateful to the numerous individuals who supported me, enabling me to successfully complete my degree. I am especially thankful to my colleagues, Dr. So-Dam Lee and Dr. Bo-Ram Hwang, with whom I had the privilege of working in the laboratory for six years. I am indebted to Dr. Haeng-Deung Jeong, Researcher Ji-Seon Kim from Yonsei University, Professor Min-Soo Noh, and Researcher Seok-Young Hwang from Seoul National University for their invaluable assistance in enabling me to complete my research. I am most grateful for all the assistance you have extended to me. I would also like to extend my gratitude to the four doctors from Korea University who provided solutions whenever issues arose. I would like to express my gratitude to my in-laws for their constant encouragement and support. I am also deeply thankful to my parents, who have been my role models and the greatest mentors in my life, for their unwavering love and support. Finally, I would like to express my gratitude to my greatest blessing, my wife, Hanna Kim, for her patience and unwavering support. I am truly thankful for her waiting silently, and I promise to make her even happier in the future. I would also like to express my gratitude to our new baby, Doyoon Yu, for coming into our lives and bringing us joy.

TABLE OF CONTENTS

LIST OF FIGURES

ABSTRACT

Helicobacter-mediated gastric cancer development and progression through YAP/TAZ signal regulation

Helicobacter pylori, a gastric pathogen, increases the risk of gastric cancer by inducing chronic inflammatory signaling pathways in gastric epithelial cells. *H. pylori* cytotoxin-associated protein A (CagA) plays a critical role in the development of human gastric cancer. Overexpression of YAP/TAZ, a component of Hippo signaling, and dysregulation of the pathway reportedly induces tumorigenesis and promotes cell proliferation and resistance to apoptosis. However, the role of YAP/TAZ in *Helicobacter*-mediated gastric carcinogenesis has not been fully investigated. We have found that YAP contributes more to the development of human gastric cancer than does TAZ based on a single-cell analysis of human gastric tissue and a publicly available database (The Cancer Genome Atlas). YAP overexpression induces expression of CDX2, a marker of intestinal epithelial metaplasia, and confers cell motility through intracellular rearrangement of the binding protein ZO-1. OTUB2, a deubiquitinating enzyme, inhibits YAP degradation and influences its nuclear translocation and gastric carcinogenesis. To further investigate the contribution of YAP/TAZ to chief cell transdifferentiation during *Helicobacter*-mediated gastric spasmolytic polypeptide-expressing metaplasia (SPEM), we infected Mist1-creERT2 $^{Cre/+}$; YAP / TAZ $^{fl/fl}$ knockout mice with *H. felis*. The knockout mice exhibited a remarkable resistance to chief-cell differentiation, oxyntic atrophy, inflammatory changes and development of SPEM in response to *H. felis* infection. Administration of recombinant OTUB2 to wild-type mice promoted metaplastic changes, whereas pretreatment of mice infected with *H. felis* with an OTUB2 inhibitor effectively prevented these changes. YAP/TAZ therefore appears to play a pivotal role in the development and progression of *Helicobacter*-mediated gastric cancer, and OTUB2 acts as a novel regulator of YAP by upregulating its expression in response to *Helicobacter* infection. These findings provide new insights into the role of YAP/TAZ signaling in gastric cancer development and progression.

Key words : Gastric cancer, Metaplasia, *Helicobacter*, YAP, TAZ, ZO-1, OTUB2, CagA

I. INTRODUCTION

Gastric cancer is the third leading cause of cancer-related deaths worldwide.[1,2] The molecular mechanisms underlying gastric cancer development remain poorly understood. The colonization of the human stomach by *Helicobacter pylori* and its role in causing gastric cancer are examples of the complex relationships among human cells, microbes, and the microenvironment. Specifically, cytotoxin-associated protein A (CagA), an oncoprotein injected into gastric epithelial cells via the type IV secretory system, disrupts the signal transduction in host cells through phosphorylation in the cytoplasm and releases proinflammatory cytokines such as interleukin (IL)-8.[3] Through this process, *H. pylori* may play an important role in inducing the formation, growth, proliferation, and metastasis of gastric cancer.

The development of gastric cancer progresses through several stages, including chronic superficial gastritis, atrophic gastritis, metaplasia (spasmolytic polypeptide-expressing metaplasia [SPEM] and intestinal metaplasia [IM]), dysplasia, and cancer.[4] Metaplasia refers to the reversible transformation of one differentiated cell type into another in response to chronic injury or inflammation. *Helicobacter*-induced chronic gastric mucosal damage and inflammation lead to pathological changes that initially manifest as metaplastic changes, such as IM.[5] IM is the process by which the gastric mucosa transforms into a structure resembling the intestinal epithelium. IM involves the transformation of various gastric epithelial cells into forms that exhibit characteristics of the intestinal epithelium, and it is considered an important precursor to gastric cancer. Specifically, gastric epithelial cells express CDX2, a marker of the intestinal epithelium, and transform into a phenotype resembling the intestinal epithelium.[6-8] This change promotes IM formation and can act as a potential risk factor for gastric cancer development. SPEM refers to the transformation of gastric chief cells into cells that express spasmolytic polypeptide. SPEM is considered a precursor to IM, and SPEM cells can gradually evolve into IM, making it an important intermediate step in gastric cancer development.[9] In chronic inflammation, such as in atrophic gastritis, the loss of parietal cells, which secrete gastric acid, increases gastric pH.

This environmental change promotes the growth of anaerobic bacteria and induces metaplastic changes, such as SPEM, in the gastric mucosa. SPEM cells express a spasmolytic polypeptide and can be identified by the expression of specific markers, such as GSII, MUC6, TFF2, and CD44v9.[9-11]

The Hippo signaling pathway regulates cell proliferation and survival in various species, ranging from fruit flies to mammals, and is overexpressed in most lumen malignancies. The core of the Hippo signaling pathway comprises the kinase cascades MST1/2 and LATS1/2 and two downstream effectors, the transcriptional coactivator yes-associated protein (YAP) and WW domain–containing transcription regulator protein 1 (TAZ).[12,13] In normal cells, the phosphorylation of the Hippo signaling pathway regulates cell survival by degrading YAP through cytoplasmic retention or ubiquitination. However, when YAP translocates to the nucleus because of the action of deubiquitination enzymes or the dysregulation of the Hippo signaling pathway, it acts as a coactivator by binding to sequence-specific transcription factors containing TEAD domains, promoting the expression of genes important for cell proliferation, apoptosis, and migration, such as CTGF, CYR61, and ANKRD1.[14-16] Recent evidence indicates that the activation of YAP/TAZ through deubiquitination can promote cancer stemness and metastasis[17,18] and suggests that YAP/TAZ mediates the Hippo signaling pathway and crosstalk with various intracellular signals. Specifically, polyubiquitin chains linked through lysine 63 (K63) play a nondegradative role.[19] The deubiquitinating enzyme OTUB2 can be poly-SUMOylated at lysine 233 by ubiquitin-like small ubiquitin-related modifier (SUMO) proteins, and deubiquitinated YAP promotes tumor growth, invasion, and metastasis.[17,20]

Intercellular junctions are critical structural components that connect cells, primarily tight junctions and adherens junctions.[21] Tight junctions are located at the apical end of cell–cell connections and play a key role in the organization of epithelial polarity and maintaining barrier function. These junctions are predominantly composed of proteins such as claudin, occludin, and zonula occludens protein 1 (ZO-1).[21-24] ZO-1, essential for tight junction integrity, directly interacts with actin filaments and stably localizes at cell–cell contact

points, maintaining intercellular adhesion.[25] The disruption of tight junctions is commonly observed in various cancers, including gastric cancer, and is considered a critical mechanism that drives tumor cell invasion and metastasis. In gastric cancer, low ZO-1 expression impairs mucosal healing, promoting the spread and invasion of cancer cells. Furthermore, diminished transcription and expression of ZO-1 in patients with inflammatory bowel disease can lead to functional impairment of the intestinal mucosa, worsening disease progression.[24] The colocalization of ZO-1 and YAP at the cell membrane is crucial for tight junction assembly, functioning as a barrier that regulates the movements of electrolytes and water.[21,23] The interaction between ZO-1 and YAP may influence the phenotypic characteristics of cancer cells, promoting tumor progression and metastasis. In addition to its structural role, ZO-1 suppresses tumor metastasis and regulates cell proliferation and migration, playing a pivotal role in cancer development.[22,26,27]

In mouse models, *H. felis* was reported to be more suitable than *H. pylori* for studying the influence of gastric inflammation on tumorigenesis.[28] *H. felis,* which does not express CagA or VacA, induces chronic infection and inflammation in well-characterized mouse models.[29] It can induce gastric mucosal lesions similar to human tissue changes. To determine the possible contribution of YAP/TAZ to chief-cell transdifferentiation during *H. felis*-mediated gastric mucosal changes, YAP/TAZ was deleted in chief cells using the tamoxifen/Cre-loxP system. In this study, *H. felis*-mediated gastric carcinogenesis was induced in YAP/TAZ-knockout and wild-type (WT) mice, and the role of YAP in the development of gastric preneoplastic metaplasia was elucidated.

In our previous study, we reported a single-cell transcriptome analysis that classified specific cell types within the gastric glands.[30] In the present study, the expressions of YAP/TAZ and related genes at the single-cell level in gastric tissues were confirmed, and deubiquitination genes were identified through the transcriptome analysis of *H. pylori*-infected AGS cells. The main aim of this study was to elucidate the mechanisms underlying gastric cancer development and progression, with a focus on the role of *H. pylori* in

mediating YAP signaling in gastric cell lines, patient-derived organoids, and mouse models. Additionally, we aimed to investigate how precursor states, such as metaplasia, contribute to gastric cancer progression and identify biomarkers that regulate YAP signaling in gastric cancer.

II. MATERIALS AND METHODS

1. Human sample and prognosis analysis

Tissue specimens, including normal, IM, and gastric cancer tissues, were obtained from patients with gastric cancer at Severance Hospital (IRB nos. 4-2011-0149 and 4-2013-0880). All patient samples were collected with informed consent. Furthermore, the overall survival duration and mRNA levels of patients with gastric cancer were evaluated based on the expression levels of YAP, TAZ, and OTUB2 from publicly available data using the Gene Expression Profiling Interactive Analysis platform (http://gepia2.cancer-pku.cn). The expression levels of YAP, TAZ, and OTUB2 in various tumors and their adjacent tissues were evaluated through analysis of the TIMER2.0 database (http://timer.cistrome.org).

2. Cell culture and bacteria

AGS (CRL-1739, ATCC, USA), AGS-LUC2 (CRL-1739-LUC2, ATCC), MKN74 (80104, KCLB, Korea), N87 (CRL-5822, ATCC), KATOIII (HTB-10, ATCC) gastric cancer cells, Caco-2 (HTB-37, ATCC) colon cancer cells, and HEK293T (CRL-11268, ATCC) kidney cells were cultured in RPMI-1640 medium (SH30027.01, HyClone, USA) or Dulbecco's Modified Eagle Medium (SH30243.01, HyClone), supplemented with 10% fetal bovine serum (FBS, Thermo Fisher Scientific, MA, USA) and 1% penicillin–streptomycin sulfate (Thermo Fisher Scientific). All cultures were maintained in a 37°C incubator with 5% CO_2. *H. pylori* strains 60190 (CagA+, 49503, ATCC), ΔCagA (CagA-), and *H. felis* (49179, ATCC) were cultured on agar plates containing 10% horse serum at 37°C under a microaerobic atmosphere maintained with the Campy Container system (BBL, USA). *H. pylori* ΔCagA strains were kindly donated by Professor M. Hatakeyama (University of Tokyo, Japan). For infection, the bacteria were harvested in Dulbecco's phosphate-buffered saline (PBS, pH 7.4) and added to the host cells at a multiplicity of infection (MOI) of 100, with an optical density at 600 nm (OD600). As a control, PBS was added to the cells and incubated for the same period.

3. Mouse preparation

In this study, 8–10-week-old C57BL/6J mice were used in all experiments. Mist1-creERT2 $^{Cre/+}$mice were generated through standard embryonic stem cell targeting, and the complete Mist1 coding region was replaced by the CreERT2 coding region. In Mist1-creERT2 $^{Cre/+}$; YAP $^{fl/fl}$; TAZ $^{fl/fl}$ mice, Cre recombinase was activated by subcutaneous injection of tamoxifen (5 mg in 0.1 mL of corn oil) every other day for a total of three doses. During the experiments, the mice were housed in a temperature-controlled room on a 12-h light/dark cycle and had free access to regular mouse chow and water. The care, maintenance, and treatment of the animals followed protocols approved by the Institutional Animal Care and Use Committee of the Department of Experimental Animal Science at Yonsei University (IACUC-2022-0314). YAP $^{fl/fl}$; TAZ $^{fl/fl}$ mice were purchased from The Jackson Laboratory (030532, Jax, USA), and Mist1-creERT2 mice were donated by Professor Ki Taek Nam (Yonsei University, South Korea).

4. Establishment of gastric organoids

Gastric organoid samples were collected from patients diagnosed with and treated for gastric cancer at the Yonsei University Severance Hospital between 2018 and 2022, and stomach tissue samples were provided by the Yonsei University College of Medicine Severance Hospital after obtaining prior approval from the Ethics Committee (IRB No. 4-2018-0676). To process the gastric tissues obtained through gastroscopy, the biopsied tissue samples were first washed three times with Dulbecco's PBS and then reacted in a dissociation buffer at room temperature for 15 min, followed by vigorous pipetting using a 1-mL tip to separate any clumped tissue into smaller fragments. Thereafter, the tissue was washed three additional times with Dulbecco's PBS, and the remaining pellet was passed through a strainer to obtain small-sized cells. To form organoids, small-sized stomach cells were combined with Matrigel at a ratio of 10 glands per 20 μL. The mixture was then dispensed into 48-well plates, where it was cured in an incubator at 37°C for 10 min. After

curing, the prepared culture medium was added, and this medium was changed every 3 days. The culture medium consisted of advanced DMEM/F12 supplemented with penicillin, streptomycin, 10 mmol/L HEPES (Invitrogen, MA, USA), Glutamax (Invitrogen), 1xB27 (Invitrogen), and 1 mM N-acetylcysteine (Sigma-Aldrich, MO, USA), along with various growth factors, including epidermal growth factor (EGF) at 50 ng/mL (Invitrogen), Noggin conditioned medium at 10%, R-spondin1 conditioned medium at 10%, Wnt conditioned medium at 50%, FGF10 at 200 ng/mL (Peprotech, NJ, USA), gastrin at 1 nM (Tocris, UK), and TGFβi at 2 μM (A-83-01, Sigma-Aldrich), as well as the optional ingredient of nicotinamide at 10 mM (Sigma-Aldrich), and 10 μM RHOKi (Y-27632, Sigma-Aldrich) was added after dispensing the Matrigel. The gastric organoid culture protocol was established based on a published study.[31]

To convert the organoids to a 2D format, approximately 2×10^5 to 2.5×10^5 cells, derived either directly from freshly isolated glands or from 3D organoids, were seeded into collagen-coated Transwell inserts (15 μg/cm²) and placed in 24-well plates containing 200 μL of culture medium. The space between the filters and wells was filled with 400 μL of the culture medium. This setup was maintained at 37°C in a humidified incubator with 5% CO_2. On day 3, air–liquid interface cultures were initiated by removing the medium above the cells from the well inserts, and 500 μL of the medium beneath the filter was changed twice a week. The composition of the 2D organoid (mucosoid) medium was similar to that of the 3D organoid medium, containing advanced DMEM/F12 supplemented with penicillin, streptomycin, 10 mmol/L HEPES (Invitrogen), Glutamax (Invitrogen), 1xB27 (Invitrogen), and 1 mM N-acetylcysteine (Sigma-Aldrich), supplemented with growth factors, including EGF at 20 ng/mL (Invitrogen), Noggin at 150 ng/mL (Peprotech), 25% R-spondin1 conditioned medium, 50% Wnt conditioned medium, FGF10 at 150 ng/mL (Peprotech), gastrin at 10 nM (Tocris), TGFβi at 1 μM (A-83-01, Sigma-Aldrich), and nicotinamide at 10 mM (Sigma), with 7.5 μM RHOKi (Y-27632, Sigma-Aldrich) added and removed after 3 days. The 2D organoid culture protocol was established based on published study.[32] *H. pylori* infection in 2D organoids was initiated on day 7 of 2D organoid

generation, with bacterial counts determined by measuring the optical density at 600 nm (MOI = 1:200). The infections were conducted on filters using 30 μL of PBS for 2 h to 3 days.

5. *H. felis*-infected mouse models

YAP $^{fl/fl}$; TAZ $^{fl/fl}$control mice and Mist1-creERT2 $^{Cre/+}$; YAP $^{fl/fl}$; TAZ $^{fl/fl}$ knockout mice were used to establish the SPEM model with *H. felis* infection. *H. felis* was cultured under microaerobic conditions in a Brucella broth (211088, BD Biosciences, USA) containing 10% FBS (Cytiva, MA, USA) at 37°C using the Campy Container system (BBL, USA). Eight-week-old mice fasted for 12 h and were treated with 200 μL of *H. felis* (5×10^{8} colony-forming units/mL) three times at 2-day intervals. The mice were sacrificed at 8 weeks postinfection, and stomach samples were harvested and fixed in 4% paraformaldehyde for histopathological analysis. Hematoxylin–eosin staining for YAP/TAZ or in situ hybridization was performed on paraffin-embedded tissues.

6. Bioinformatic analysis

QuantSeq 3′ mRNA-Seq Library Prep Kit FWD was used for transcriptome profiling of AGS gastric cancer cell lines. To identify differentially expressed genes (DEGs) between the groups, raw data were compiled, standardized, and analyzed using the gene-level robust multiaverage approach. The null hypothesis was that there was no difference between the groups, and significant DEGs were determined using independent t-tests and fold-change in expression level. Gene enrichment and functional annotation analysis for the significant probe list were performed using Gene Ontology (www.geneontology.org). Data analyses and visualization of the DEGs were performed with ExDEGA (Ebiogen, South Korea). As directed by the manufacturer, GSEA was performed using gene set files, expression dataset files, and GSEA v4.0.3 (Broad Institute, MA, USA). The GSEA browser provided the gene sets for download. The QuantSeq 3′ mRNAseq transcriptome dataset for this study was deposited in the Gene Expression Omnibus (GEO) database (GSE275727).

7. Single-cell analysis of the RNA-seq data of human gastric cancer

For the analysis of the expression levels in human gastric cancer, public scRNA-seq data (GSE150290) were used to reanalyze samples from the normal tissues of five patients without cancer and paired cancerous and adjacent tissues from 24 patients with gastric cancer. In summary, a gene-count matrix was constructed from the fastq files mapped to the GRCh38 reference genome using the Cell Ranger software (v7.0.0) provided by 10× Genomics. Following the previous approach, low-quality cells were filtered based on the following criteria: RNA counts >20,000, RNA feature counts <200 or >2,000, and mitochondrial gene and hemoglobin gene percentages >30% and 10%. The remaining cells were normalized and clustered using the unsupervised clustering method through the FindClusters function (resolution = 0.3) in the Seurat R package (v5.0.0). Clusters were annotated by manually inspecting DEGs compared with previously defined cell type markers. The single-cell analysis consisted of the GSE150290 data previously deposited by our research team in the GEO database. Single-cell quality control and data preprocessing were performed in the same manner as in our previous study.[30]

8. Western blotting

Cells were collected and resuspended in RIPA buffer, which contained 25 mmol/L Tris-Cl (pH 7.4), 0.15 mol/L NaCl, 1% NP40, 0.1% sodium dodecyl sulfate (SDS), 1% sodium deoxycholate, and 1 mmol/L EDTA, along with a cocktail of protease and phosphatase inhibitors (P3300, GenDEPOT, USA). The protein concentrations in the lysates were measured, and an SDS sample buffer consisting of 62.5 mM Tris-Cl (pH 6.8), 2% SDS, 10% glycerol, β-mercaptoethanol, and 0.002% bromophenol blue was added. The samples were then heated at 95°C for 5 min. Proteins were separated by SDS–polyacrylamide gel electrophoresis (PAGE) using 7% or 10% gels and subsequently transferred to Immobilon-FL polyvinylidene fluoride membranes (IPFL00010, Merck Millipore, MA, USA). Primary antibodies were incubated overnight at 4°C with gentle agitation, and the signal was

developed using SuperSignal West Pico PLUS Chemiluminescent Substrate (34580, Thermo Fisher Scientific) in the dark. Specific antibodies are listed in Supplementary Material 1.

9. Cell fractionation

AGS cells were infected with *H. pylori* 60190 (CagA-positive) and *H. pylori* ΔCagA (CagA-negative). Following the manufacturer's instructions, nuclear-cytoplasmic fractionation was performed 5 h following infection using the NE-PER Nuclear and Cytoplasmic Extraction Reagent Kit (78833, Thermo Fisher Scientific).

10. RNA extraction and reverse-transcription quantitative PCR

RNA was extracted from the tissues, cells, and organoids using the QIAzol lysis reagent (QIAGEN 79306) following the manufacturer's instructions. cDNA was synthesized with 1 μg of RNA using Maxime RT PreMix (25081, Intronbio, Korea). Quantitative PCR amplification was conducted with SYBR Green (CMQSR1000, Cosmogenetech, Korea) according to the manufacturer's guidelines. The specific primers utilized in this study are detailed in Supplementary Material 1.

11. ELISA

IL-8 levels were quantified using a direct-sandwich ELISA method, with each test sample analyzed in quintuplicate. Human CXCL8/IL-8 was obtained using the DuoSET (DY208-05, R&D Systems, MN, USA) and the DuoSET Ancillary Reagent Kit (DY008, R&D Systems). Optical absorbance was measured at 450 nm with a VersaMax microplate reader, and the lower sensitivity limit of this ELISA was 20 pg/mL.

12. Scanning and transmission electron microscopy

For scanning electron microscopy **(**SEM), 2D organoid specimens were fixed for 24 h in Karnovsky's fixative, which consists of 2% glutaraldehyde and 2% paraformaldehyde in a

0.1 M phosphate buffer (pH 7.4). Subsequently, the specimens were washed twice for 30 min each in a 0.1 M phosphate buffer. A Critical Point Dryer (LEICA EM CPD300) was used to process the specimens after they had been postfixed with 1% OsO4 for 2 h and dehydrated in a sequence of increasing ethanol concentrations (from 50% to 100%). An ion sputter coater (LEICA EM ACE600) was used to coat the specimens with platinum, and a field-emission scanning electron microscope (MERLIN, ZEISS) was used for observation. For transmission electron microscopy (TEM), 2D organoid specimens were post-fixed with 1% OsO4 in a 0.1 M phosphate buffer for 2 h after being fixed for 12 h in 2% glutaraldehyde and 2% paraformaldehyde dissolved in a 0.1 M phosphate buffer (pH 7.4). The samples were then dehydrated using increasing ethanol concentrations (50%, 60%, 70%, 80%, 90%, 95%, and 100%) and infiltrated with propylene oxide for 10 min at each concentration. Afterward, they were polymerized using a Poly/Bed 812 kit (Polysciences) at 65°C for 12 h in an electron microscope oven (TD-700, DOSAKA, Japan). Using a diamond knife, the resultant blocks were placed on an ultramicrotome and sliced into semi-thin sections measuring 200 nm. These sections were then stained with toluidine blue and examined under an optical microscope. An ultramicrotome was then used to cut the regions of interest into 80-nm thin sections, which were then placed on copper grids, double-stained with 3% uranyl acetate for 30 min and 3% lead citrate for 7 min, and imaged using a Megaview III CCD camera (Soft Imaging System, Germany) and a transmission electron microscope (JEM-1011, JEOL, Japan) set to an acceleration voltage of 80 kV.

13. Transepithelial electrical resistance (TEER)

To measure the TEER according to the 2D organoid cell density, the electrical resistance values of the cell layer and culture medium portions were measured using EVOM2 (WPI, UK). To obtain the resistance of an actual 2D organoid epithelium, the blank resistance must be measured and then subtracted from the overall resistance reading.

14. Small-interfering RNA (siRNA) transfection

Bioneer Co. Ltd. created the control and YAP siRNAs. These were the siRNA duplexes: The first YAP siRNA sense strand is CAG AAG AUC AAA GCU ACU U=TT(1-AS). The first antisense strand is AAG UAG CUU UGA UCU G=TT(1-AA). The second sense strand is AGA ACC GUU UCC CAG ACU A =tt(3-AS). The second antisense strand is UAG UCU GGG AAA CGG UUC U=tt(3-AA). The siRNA for OTUB2 was purchased as a premade product from Santa Cruz (sc-76016). Using Lipofectamine RNAiMax, 20 nM siRNA was transfected into AGS and MKN74 cells in accordance with the manufacturer's instructions (13778-150, Invitrogen).

15. Plasmid transfection

Following the manufacturer's instructions, Lipofectamine 2000 (11668-019, Invitrogen) was used to transfect AGS and MKN74 cells with each construct. Sample of pEGFP-C3-hYAP1 (#17843) was bought from Addgene. Full-length structures of CagA (AF202923) and EPIYA PR mutants were supplied by Professor M. Hatakeyama of the University of Tokyo (Japan). The media were swapped out for a new medium 6 h after transfection. Cells were used 24 h after transfection for every assay.

16. Electroporation

YAP-EGFP vector and YAP siRNA were delivered to gastric organoids by electroporation of NEPA21 (Nepagene, Japan) according to the manufacturer's instructions.

17. YAP-TEAD luciferase assay

Cells were transduced at an MOI of 5 using a commercial lentiviral construct incorporating a luciferase reporter for TEAD activity (TEAD Luciferase Reporter Lentivirus, 79833, BPS Bioscience, USA). A commercial kit (Steady-Glo Luciferase Assay System, E2510, Promega, USA) was used to assess luciferase activity, which was then normalized to the cell number.

18. Ubiquitination and SUMOylation assay

AGS cells were transfected with His-Ub for 24 h and then infected with *H. pylori* 60190 and ΔCagA for 5 h. YAP and OTUB2 were immunoprecipitated using Protein A/G PLUS agarose beads, and the immunoprecipitates were subsequently separated on 10% SDS–PAGE gels. Deubiquitinated YAP and SUMOylated OTUB2 were detected using an anti-Ub antibody (sc-8017, Santa Cruz, USA) and anti-SUMO2/3.

19. Lentiviral transduction and generation of stable cell lines

Premade lentiviral short-hairpin RNA (shRNA) constructs and a negative control consisting of a construct identical to the vector system (pLKO.1) were purchased from Addgene (shYAP#1, 42540; shYAP#2, 42541; shControl, 8453). Lentiviral particles were produced *in vitro* using a 3rd Generation Packaging System Mix (LV053, abm, USA) and lentipectin (G074, abm). According to the manufacturer's protocol, cell supernatants were harvested 48 h after transfection in HEK293T cells and used to infect cells or stored at −80°C. Puromycin (2 μg/mL) was used for 48 h after lentiviral infection to select AGS and MKN74 cells that stably expressed the shRNA constructs. A Western blot was used to identify and validate the positive clones.

20. Xenograft mouse model

5×10^6 AGS-shRNA (YAP#1, YAP#2, and control cells) and 8×10^6MKN74-shRNA (YAP#1, YAP#2, and control cells) were subcutaneously injected into each mouse's hind limbs for the *in vivo* xenograft study. The mice were raised at the Yonsei University College of Medicine in a pathogen-free animal facility. All studies followed the protocols authorized by the Institutional Animal Care and Use Committee (IACUC no. 2023-0047). Every 3–5 days, the tumor size was measured with calipers, and the formula (length × width ^{2})/2 was used to determine its volume. Tumors were removed for photography when the mice were slaughtered 60–110 days post-injection. Each group's tumor tissues were stored in liquid nitrogen. For immunohistochemistry and hematoxylin and eosin (H&E)

staining, portions of the tissue were preserved in 10% formaldehyde.

21. Immunostaining and in situ hybridization

Formalin-fixed paraffin-embedded (FFPE) slides were deparaffinized and then rehydrated in a declining graded sequence of ethanol (100%, 90%, and 70%) for immunostaining. A cooker was used to incubate the slides at high pressure after they were submerged in an antigen-retrieval solution (S169984-2, Dako, Denmark). To inhibit endogenous peroxidase activity, the slides were treated in 3% hydrogen peroxide for 30 min after cooling on ice for 1 h. After two PBS washes, the slides were incubated for 1–2 h at room temperature in a humidity chamber with serum-free protein blocks (X0909, Dako). The mouse tissue was treated with a mouse-on-mouse (vector) reagent before antibody application. Primary antibodies were incubated on the tissues for an entire night at 4°C. After three PBS washes, the specimens were incubated for 15 min at room temperature in either HRP-conjugated anti-mouse secondary antibodies (Dako) or HRP-conjugated anti-rabbit secondary antibodies (Dako). Mayer hematoxylin (Dako) was employed for nuclear staining in the immunohistochemical analysis, whereas diaminobenzidine was used for signal expression. For immunofluorescence, Texas Red dye (Invitrogen) and fluorescein isothiocyanate (FITC, Invitrogen)-, Cy3 (Invitrogen)-, and Cy5 (Invitrogen)-conjugated secondary antibodies were used to detect each primary antibody derived from various species. 6-diamino-2-phenylindole (DAPI, Sigma, Japan) was used for nuclear staining. The LSM 770 (Zeiss, Germany) and EVOS-M5000 (Thermo Fisher Scientific) microscopes were used for confocal and immunofluorescence imaging, respectively.

H. felis-specific probes and an RNAscope 2.5 HD detection kit were acquired from Advanced Cell Diagnostics (ACD, USA) and utilized in accordance with the manufacturer's instructions for in situ hybridization. Briefly, a ready-to-use protease, hydrogen peroxide, and a target retrieval solution were used as pretreatments for the deparaffinized FFPE slides. In a HybEZ oven (ACD, USA), prewarmed probes were placed on slides and incubated for 2 h at 40°C. After signal amplification, Fast Red dye

development was conducted. Counterstaining was performed with Mayer hematoxylin.

22. Intraperitoneal injection of recombinant OTUB2 into WT mice

To investigate the effects of exogenous recombinant OTUB2 (rOTUB2, 13177-H07E, Sino Biological) on SPEM development in WT mice, rOTUB2 was administered intraperitoneally at doses of 2 μg/100 μL every other day for 7 days. Stomach samples were collected from the mice 8 weeks after the last injection. The control mice were treated with the same PBS volume.

23. Injection of OTUB2 inhibitors to control metaplastic changes in *H. felis*-infected mice

The effects of the OTUB2 inhibitor (LN5P45, HY-149482, Medchem) on *H. felis*-mediated SPEM were assessed. The concentration of the OTUB2 inhibitor for *in vivo* studies was determined based on its *in vitro* IC50 value of 2.3 μM. Owing to variations in bioavailability, metabolism, and distribution, the drug dose required in mouse experiments can differ significantly from that used in cell line studies, necessitating 10- to 100-fold higher doses *in vivo*.[33] Consequently, 2.5 mg/100 μL of LN5P45, approximately 40 times the IC50, was intraperitoneally administered to the mice. WT mice were pretreated with the OTUB2 inhibitor every other day for 7 days before infection with *H. felis*, followed by an 8-week infection duration.

24. Statistical analysis

Statistical analyses were performed using GraphPad Prism version 10.3.1 (GraphPad Software Inc., La Jolla, CA). Significance was determined using a two-tailed unpaired Student's t-test for comparisons between two groups, or a one-way or two-way analysis of variance with Tukey's multiple comparisons for comparisons involving multiple groups. All data are presented as means ± SEM. $P < 0.05$ was considered significant.

III. RESULT

1. YAP/TAZ expression in human gastric cancer

The GEPIA tool was used to measure YAP/TAZ (mRNA) expression in tumors and adjacent normal tissues of gastric cancer (STAD). YAP was significantly increased in tumor tissues compared with normal tissues, whereas TAZ was not (Figure 1A). Furthermore, YAP/TAZ expression in various tumors was confirmed by analyzing the TIMER 2.0 database. Similarly, YAP was significantly upregulated in gastric cancer, whereas TAZ (WWTR1) was not (Supplementary Figure 1A). To analyze the expression levels of YAP/TAZ in human gastric cancer, public scRNA-sequencing data (GSE150290) were used to reanalyze samples from normal tissues of five patients without cancer patients and paired cancerous and adjacent tissues from 24 patients with gastric cancer. A t-distributed stochastic neighbor embedding (t-SNE) plot from human gastric single-cell analysis showed higher concentrations of YAP- and TAZ-positive cells in patients with IM, intestinal gastric cancer (IGC), and diffuse gastric cancer (DGC) compared with those with chronic superficial gastritis (CSG) (Figure 1B–1E). The intensity of YAP expression was higher than that of TAZ in gland mucous cells, pit mucous cells, and chief cells as the gastric cancer progressed. Conversely, TAZ was expressed at higher levels in the endothelial cells (Figure 1F). Accordingly, YAP may play a relatively more important role than TAZ in epithelial metaplasia and gastric carcinogenesis. Immunohistochemical staining showed a progressive increase in YAP- and TAZ-positive cells from IM to gastric cancer, with minimal YAP/TAZ expression in the CSG. A strong YAP/TAZ expression was detected in the nucleus of gastric cancer cells (Figure 1G), signifying that YAP/TAZ may function as an intranuclear signaling molecule. Furthermore, the expression of the tight junction protein ZO-1 was significantly and progressively decreased from CSG to gastric cancer, and this decrease was negatively correlated with the expansion of YAP-positive cells in gastric lesions (Figure 1H). Western blotting confirmed the basal expression level of YAP/TAZ in various gastric cancer cell lines (AGS, N87, KATOIII, MKN45, and MKN74), colorectal cancer cell line (Caco2), and kidney epithelial cells (293T) (Figure 1I).

YAP/TAZ expression was significantly increased in AGS and MKN74 cells upon *H. pylori* infection (Figure 1J). Based on these results, AGS and MKN74 cells were used for the next *in vitro* experiments. The experimental data for MKN74 cells are presented in Supplementary Figure 6.

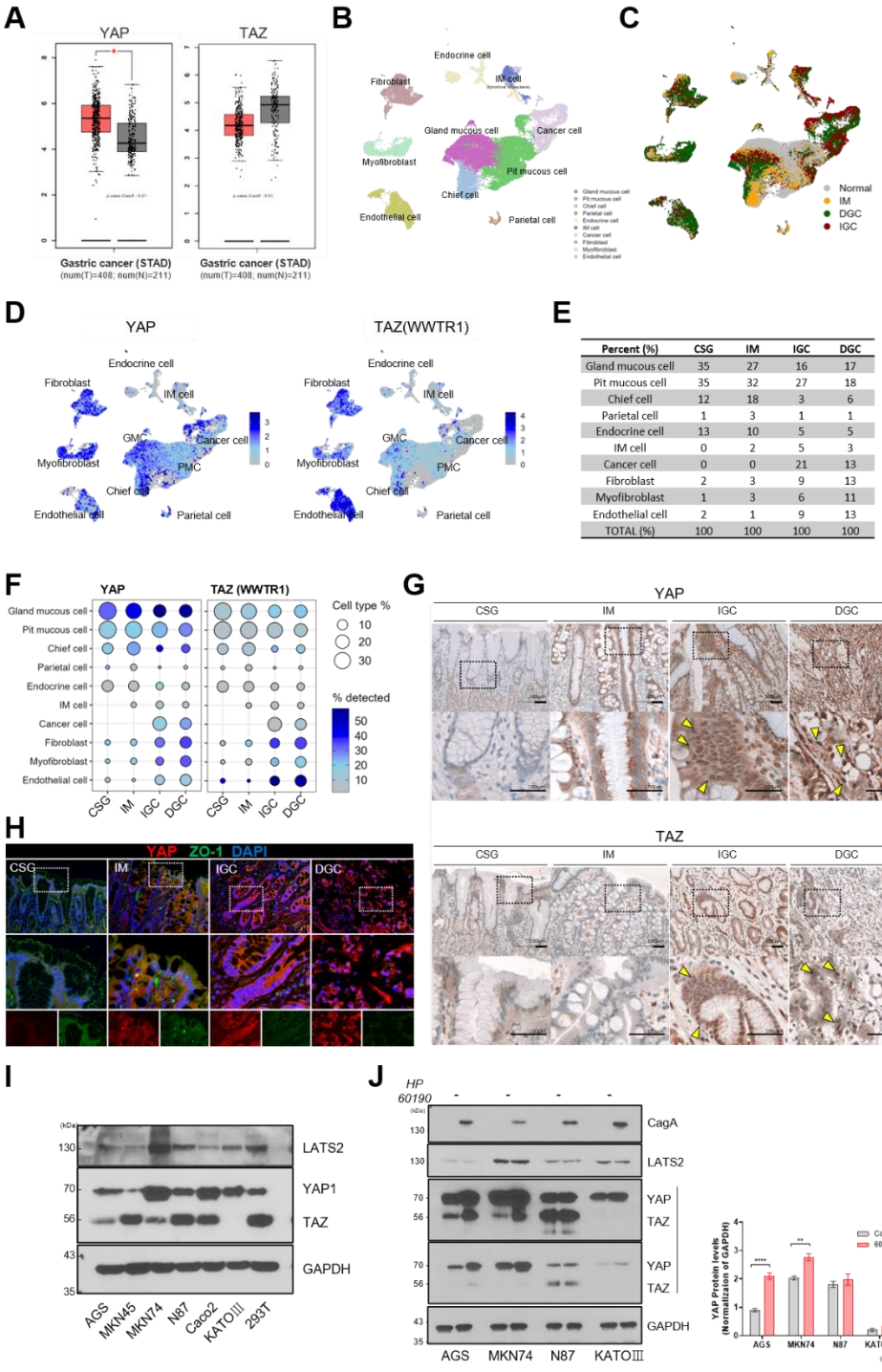

Percent (%)	CSG	IM	IGC	DGC
Gland mucous cell	35	27	16	17
Pit mucous cell	35	32	27	18
Chief cell	12	18	3	6
Parietal cell	1	3	1	1
Endocrine cell	13	10	5	5
IM cell	0	2	5	3
Cancer cell	0	0	21	13
Fibroblast	2	3	9	13
Myofibroblast	1	3	6	11
Endothelial cell	2	1	9	13
TOTAL (%)	100	100	100	100

Figure 1. Expression of YAP/TAZ in human gastric cancer tissues and gastric cell lines. (A) Analysis of YAP/TAZ expression in gastric cancer (STAD) and adjacent normal tissues using the Gene Expression Profiling Interactive Analysis Database (Tumor: 408, Normal: 211). Statistical analysis was performed using the Mann–Whitney U test: *P < 0.05. GEPIA: http://gepia.cancer-pku.cn/. (B) t-SNE map of 48,670 single cells filtered from adjacent noncancerous and cancerous tissues. (C) t-SNE map showing the distribution of single cells in chronic superficial gastritis (CSG), intestinal metaplasia (IM), intestinal-type gastric cancer (IGC), and diffuse-type gastric cancer (DGC) tissues. (D) t-SNE plot showing YAP/TAZ gene expression in 10 gastric epithelial cell types established by single-cell transcriptomic analysis. (E) Proportions of gastric cell types in CSG, IM, IGC, and DGC. (F) Dot plot showing YAP/TAZ expression according to the gastric lesion cell types (the color indicates expression intensity, and the dot size indicates the total amount of each cell type). (G) Immunohistochemical image of YAP and TAZ in human gastric tissues, including CSG, IM, IGC, and DGC. Scale bar = 100 μm. (H) Immunofluorescence images of YAP and ZO-1 in patient gastric tissues, including CSG, IM, IGC, and DGC. Scale bar = 250 μm. (I) Representative Western blot data demonstrating basal expression levels of Hippo signaling pathway-related genes (YAP/TAZ/LATS2) in gastric cancer cell lines (AGS, N87, KATOIII, MKN45, and MKN74), colorectal cancer cells (Caco2), and kidney epithelial cells (293T). (J) YAP/TAZ protein levels in gastric cancer cell lines (AGS, MKN74, N87, and KATOIII) infected with *H. pylori* 60190 for 5 h. Graph showing fold changes in YAP protein expression in *H. pylori* 60190 compared with the control (n = 5 per group). Statistical analysis was performed using a two-tailed unpaired Student's t-test: *P < 0.05; **P < 0.01; ***P < 0.001. All data are presented as means ± SEM. CSG, chronic superficial gastritis; DGC, diffuse type gastric cancer; IGC, intestinal type gastric cancer; IM, intestinal metaplasia; GMC, gland mucous cell; PMC, pit mucous cell

2. CagA-positive *H. pylori* induces changes in the Hippo signaling pathway, K-63 deubiquitination, and inflammatory gene expression in gastric cancer cells

When AGS cells were infected with *H. pylori* (Figure 2A) or transfected with a CagA expression vector (Figure 2B), the expression of YAP/TAZ proteins increased. In AGS cells infected with *H. pylori* 60190 (a CagA-positive strain), the expression of YAP proteins peaked at 5 h. Transcriptome analysis revealed differences in the expression patterns of Hippo signaling pathway genes (Gene Ontology: 0035329) in AGS cells, depending on the presence or absence of *H. pylori* infection (60190, ΔCagA) (Figure 2C). In *H. pylori* 60190-infected AGS cells, the expression levels of YAP, WWTR1, LATS2, SAV1, STK4, and TEAD1 were higher than those in uninfected AGS cells or cells infected with *H. pylori* ΔCagA (a CagA-negative strain). Gene set enrichment analysis (GSEA) revealed that the gene sets associated with YAP signaling and gastric cancer were positively enriched in *H. pylori*-infected AGS cells (Figure 2D and Supplementary Figure 3). To determine whether the increase in YAP expression is linked to the inhibition of protein degradation, GSEA was performed on K63-linked deubiquitination gene sets, which showed a higher enrichment score (ES) in *H. pylori* 60190 compared with *H. pylori* ΔCagA (Figure 2E). Additionally, the ES of the CXCR chemokine receptor-binding gene set was positively enriched in *H. pylori* 60190, with the expression of the proinflammatory mediator CXCL8 (IL-8 or chemokine ligand 8) being the highest among them (Figure 2F). Furthermore, IL-8 production in *H. pylori* 60190-infected AGS cells was significantly increased at 8 h compared with both uninfected cells and those infected with *H. pylori* ΔCagA, as confirmed by enzyme-linked immunosorbent assay (ELISA) (Figure 2G).

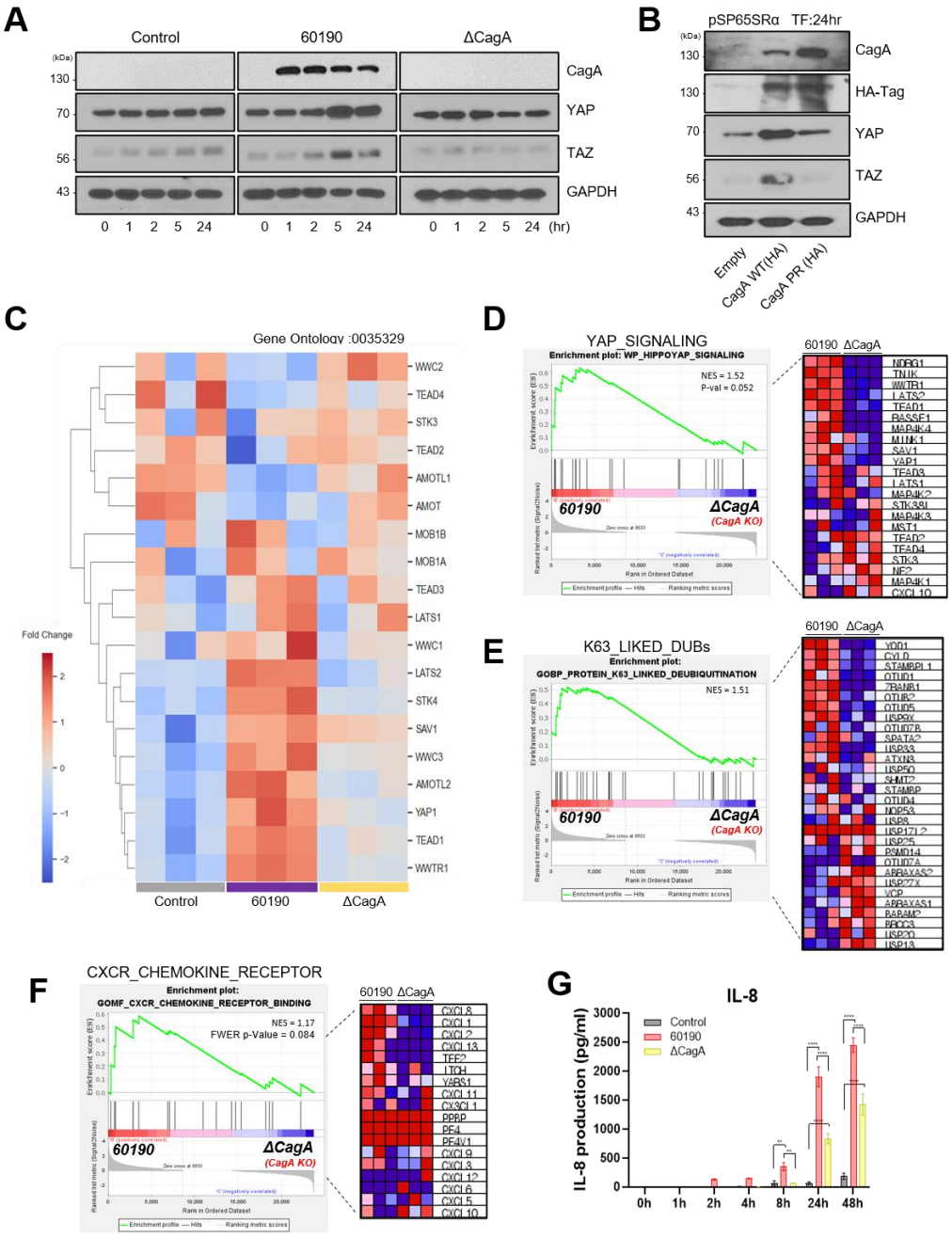

Figure 2. Alterations in the Hippo signaling pathway, K63-linked deubiquitination, and inflammatory pathways in *H. pylori*-infected AGS cells. (A) AGS cells were

infected with *H. pylori* (60190, ΔCagA) for the indicated periods, and YAP/TAZ expression was confirmed by Western blotting of harvested cell lysates. (B) AGS cells were transfected with HA-tagged CagA WT and CagA mutant expression vectors for 24 h. CagA PR indicates a tyrosine-phosphorylation mutant in the EPIYA motif. (C) Heatmap showing differentially expressed genes involved in the Hippo signaling pathway-related Gene Ontology terms (GO:0035329) in AGS cells infected with *H. pylori* for 5 h. (D) GSEA plot for YAP signaling gene signature. (60190 vs. ΔCagA). (E) GSEA plot for the K63-linked deubiquitination. (60190 vs. ΔCagA). (F) GSEA plot for the CXCR chemokine receptor-binding gene set (60190 vs. Δ CagA). (G) ELISA results for IL-8 production in AGS cells infected with *H. pylori* 60190 and ΔCagA (n = 4 per group). Statistical analysis was performed using two-way analysis of variance with Tukey's multiple comparisons: *P < 0.05; **P < 0.01; ***P < 0.001. All data are presented as mean ± SEM.

3. *H. pylori* infection induces YAP nuclear translocation and ZO-1 downregulation, promoting metaplastic changes through CDX2 overexpression

Nuclear-cytoplasmic fractionation analysis was performed to identify YAP-related changes in the subcellular locations. In *H. pylori* 60190-infected AGS cells, YAP expression levels were higher in the nucleus than in the cytoplasm, whereas p-YAP was primarily expressed in the cytoplasm (Figure 3A). Quantitative analysis of the fluorescence images also showed that a significant number of YAP proteins translocated to the nucleus in *H. pylori* 60190-infected AGS cells (Figure 3B). In *H. pylori* 60190-infected AGS cells, YAP nuclear expression was observed at 5 h. Although some YAP nuclear expression was observed in *H. pylori* ΔCagA infection, it was less prominent than that in *H. pylori* 60190 infection (Supplementary Figure 4C). This proposes that YAP overexpression and nuclear translocation are CagA-dependent. Intercellular junctions are crucial structural connections between cells, primarily tight and adherens junctions. Most tight junctions are formed by proteins such as claudin, occludin, and ZO-1.[21-24] Western blot analysis revealed that the expression of these proteins decreased during *H. pylori* infection, signifying potential

structural changes in the tight junctions (Supplementary Figures 4D and 6A). Notably, YAP proteins play a significant regulatory role in both tight junctions and intercellular junctions.[23,34,35] Quantitative reverse-transcription polymerase chain reaction (PCR) amplification (Figure 3C and Supplementary Figure 4B) and Western blot analysis (Figure 3D and Supplementary Figure 4A) showed that CagA-mediated YAP nuclear translocation was associated with ZO-1 downregulation and CDX2 overexpression. YAP overexpression led to a reduction in ZO-1 expression at the sites of cell adhesion (Figure 3E). The expression of CDX2, an intestinal-specific transcription factor, plays an important role in the progression of IM to dysplasia and gastric cancer.[6-8] Expectedly, CDX2 expression was significantly increased in *H. pylori* 60190-infected AGS cells (Figure 3F). This proposes that CagA delivery disrupts the epithelial barrier function and induce metaplastic changes in the epithelial cell lineage. The proteasome inhibitor MG132 prevented YAP degradation, leading to its accumulation and further reduction in ZO-1 (Supplementary Figure 4E).

4. YAP downregulation suppresses *H. pylori*-induced changes in tight junctions and CDX2 expression

As the transcriptional coactivator YAP localizes to the nucleus, it induces the expression of TEAD luciferase reporter genes. The TEAD luciferase reporter was activated in *H. pylori* 60190-infected AGS, whereas TEAD luciferase activity did not increase in YAP-knockout AGS cells (shYAP#1 and shYAP#2) (Supplementary Figure 5A). Western blot analysis confirmed the suppression of protein changes in CDX2 and ZO-1 in infected YAP-knockout AGS cells (Figure 3G). Immunofluorescence staining showed restored ZO-1 expression (Figure 3H) and suppressed CDX2 expression (Figure 3I) in YAP-knockout cells. Conversely, in AGS cells overexpressing YAP through the p-EGFP-C3-hYAP1 vector, the expression of ZO-1 was suppressed (Supplementary Figure 4F and 4G). Metaplastic cells do not easily progress to dysplasia in the absence of inflammatory responses.[36] In this study, YAP downregulation significantly reduced the *H. pylori*-mediated production of IL-8 (Supplementary Figure 5B), proposing that YAP expression in gastric epithelial cells is

associated with *H. pylori*-mediated inflammatory responses and promote metaplasia development. Furthermore, the effect of YAP downregulation on gastric tumorigenesis was assessed using AGS and MKN74 xenograft mouse models. Tumor growth and weight change were significantly reduced in YAP-deficient xenograft mice (Figure 3J and Supplementary Figures 5 and 6). The light intensity detected by the *in vivo* imaging system was correlated with the xenograft size (Figure 3K). YAP expression in the xenograft was reconfirmed through DAB staining (Figure 3L and Supplementary Figures 5C). Moreover, in tumors with inhibited YAP expression, CDX2 expression was reduced, and ZO-1 expression was increased (Supplementary Figure 5D).

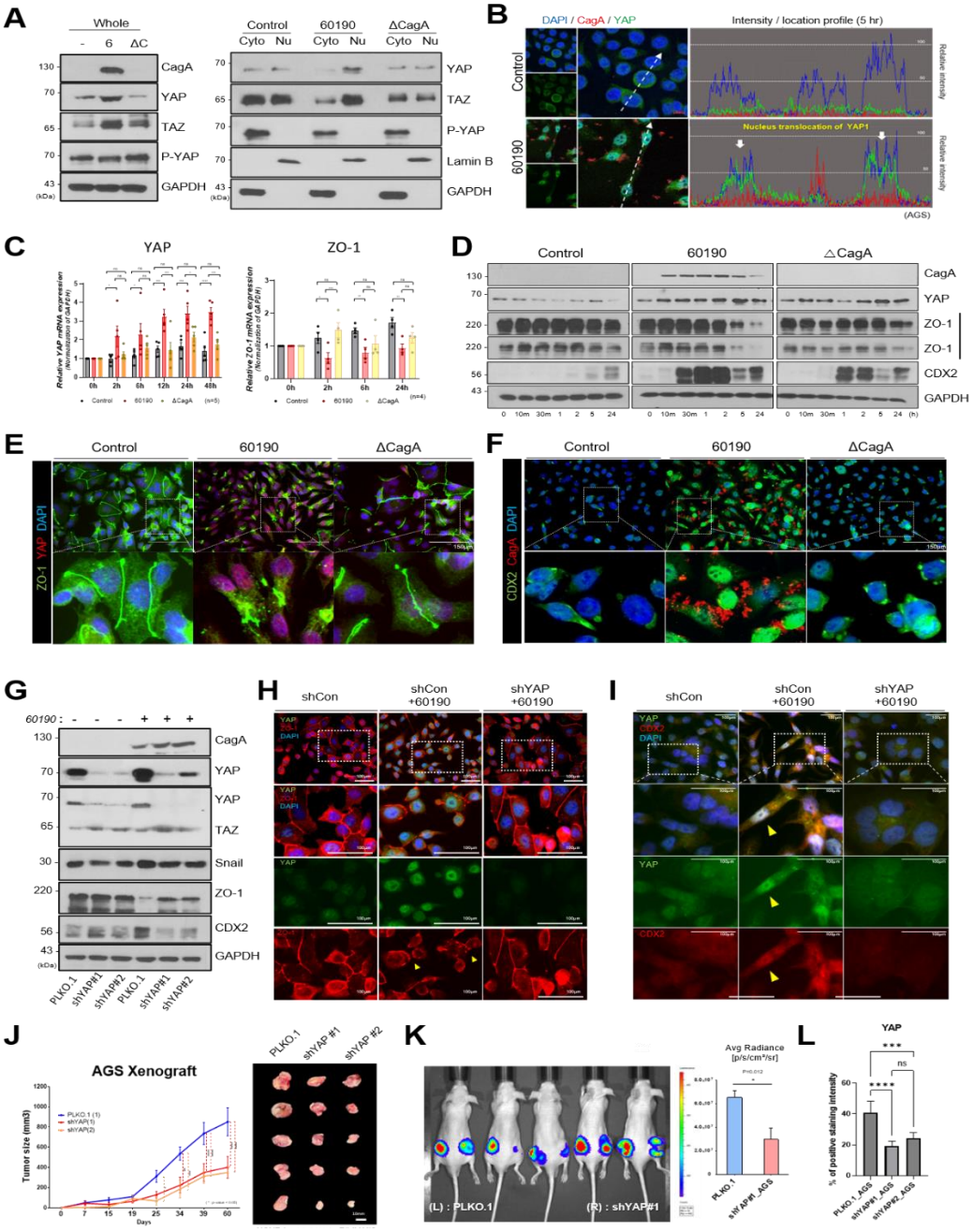

Figure 3. Tight junction disruption and intestinal metaplasia are associated with YAP nuclear translocation. (A) AGS cells were infected with *H. pylori* 60190 or ΔCagA for 5

h, followed by nuclear-cytoplasmic fractionation and Western blot analysis of cytoplasmic and nuclear extracts. (B) AGS cells were infected with *H. pylori* 60190 for 5 h, fixed, and stained for YAP and CagA. Quantitative fluorescence analysis showed YAP translocation to the nucleus. Scale bar = 50 μm. (YAP and CagA fluorescence staining images of AGS cells infected with *H. pylori* 60190 and ΔCagA for 2, 5, and 24 h are provided in Supplementary Figure 4C). (C) qRT-PCR analysis of YAP and ZO-1 mRNA levels in AGS cells infected with *H. pylori* (60190 or ΔCagA) for the indicated times. (YAP, n = 5; ZO-1, n = 4). (D) Representative Western blot data showing ZO-1 and CDX2 expression in AGS cells infected with *H. pylori* for the indicated times. (E, F) Immunofluorescence images of ZO-1 and CDX2 in AGS cells treated with control, *H. pylori* 60190, or ΔCagA for 5 h. Scale bar = 150 μm. (G) Western blot analysis of ZO-1 and CDX2 expression in YAP-silenced AGS cells. (H) Immunofluorescence images of ZO-1 and YAP in control and YAP-silenced AGS cells infected with *H. pylori* 60190 for 5 h. Scale bar = 100 μm. (I) Immunofluorescence images of CDX2 and YAP in control and YAP-silenced AGS cells infected with *H. pylori* 60190 for 2 h. Scale bar = 50 μm. (J) Tumor size after subcutaneous injection of AGS-PLKO.1 (shControl, 8453, Addgene) or AGS-shYAP (42540, 42541, Addgene) into mice (n = 5). The image on the right shows the tumor at day 60. (K) Bioluminescence images of mice injected with AGS cells (PLKO, shYAP#1), showing radiative efficiency. (L) DAB staining of YAP+ cells in AGS xenograft tumors, with quantification of YAP+ cell proportions (n = 5). Statistical analysis was performed using two-way analysis of variance with Tukey's multiple comparisons and two-tailed unpaired Student's t-test: *P < 0.05; **P < 0.01; ***P < 0.001. All data are presented as mean ± SEM.

5. OTUB2 deubiquitinates and activates YAP to promote tumor growth in *H. pylori* infection

YAP signaling is controlled by proteasomal degradation via ubiquitination, starting with inactivation by the phosphorylation of Ser127. The K63-linked deubiquitination gene

expression (GO:0070536) was profiled to investigate the regulatory mechanism for ubiquitination in *H. pylori*-infected gastric cancer cell lines, and among the 29 genes, OTUB2 was the most highly expressed (Figure 4A). In *H. pylori* 60190-infected AGS cells, mRNA and protein levels of OTUB2 were significantly upregulated (Figure 4B–4D). Furthermore, CagA activated YAP by counteracting the poly-ubiquitination of YAP proteins and subsequent proteasomal degradation (Figure 4E). OTUB2, which simultaneously binds to YAP, was excessively poly-SUMOylated (Figure 4F). Thus, OTUB2 SUMOylation may be directly involved in YAP deubiquitination. The transfection of rOTUB2 into AGS cells induced YAP expression, leading to the inhibition of ZO-1 and increased expression of CDX2 (Figure 4G). In contrast, the depletion of OTUB2 with siOTUB2 suppressed YAP expression (Figure 4H). Moreover, in the single-cell analysis, OTUB2 expression was higher in IM cells than in gastric cancer tissues (Figure 4I). Immunostaining of human gastric tissues showed a progressive increase in OTUB2-staining cells from CSG to gastric cancer, with a pattern similar to that of YAP expression (Figure 4J).

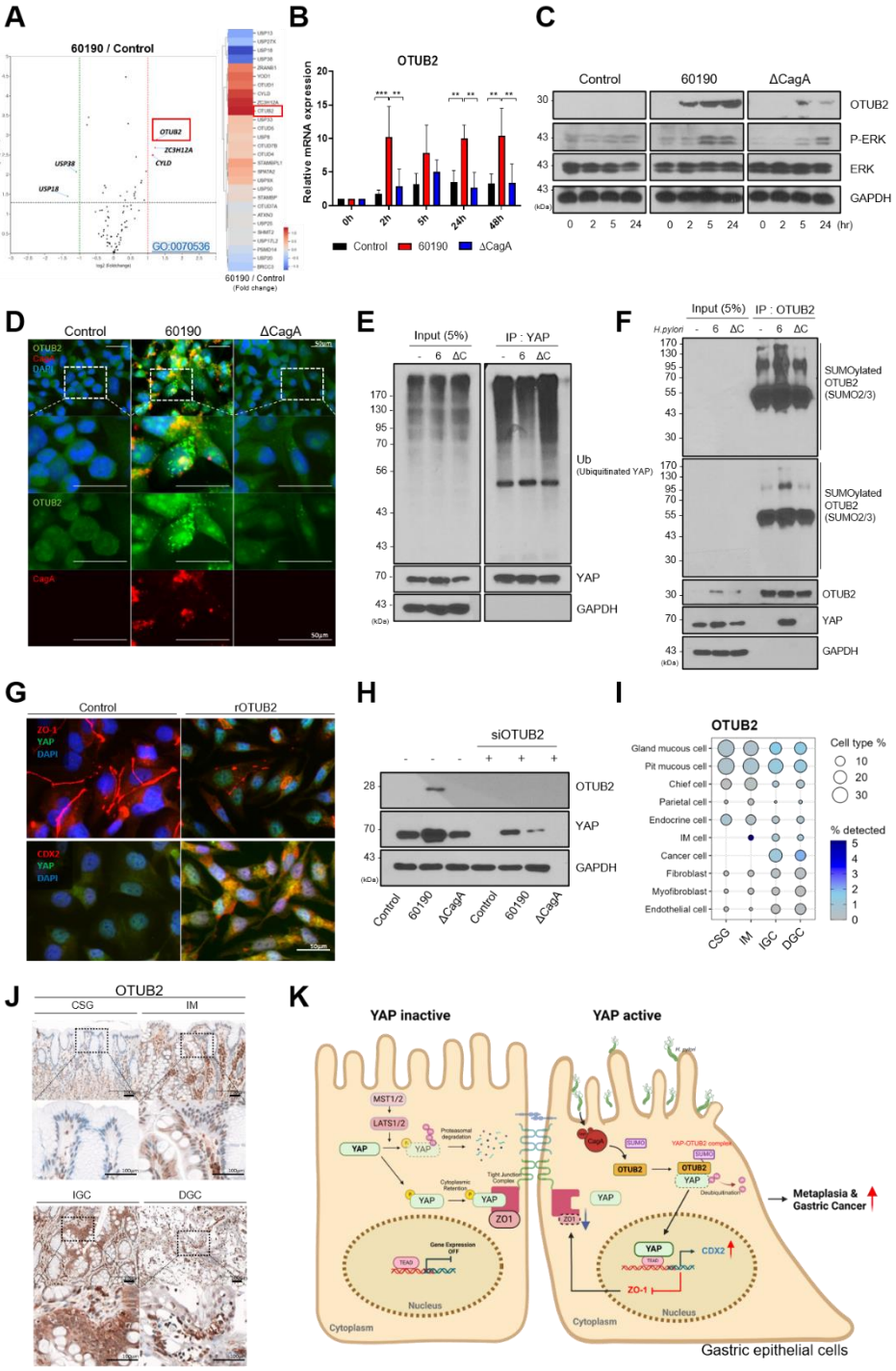

Figure 4. Function of OTUB2 (OTU deubiquitinase), a deubiquitination protein, as a novel YAP regulator. (A) Scatterplot and heatmap showing differentially expressed genes related to the protein K63-linked deubiquitination ontology term (GO:0070536) in the mRNA sequencing data of control and *H. pylori* 60190-infected AGS cells. Selected genes are highlighted. (B) qRT-PCR analysis of OTUB2 expression in AGS cells infected with *H. pylori* 60190 and ΔCagA. mRNA expression levels were normalized to GAPDH (n = 4). Statistical analysis was performed using two-way analysis of variance with Tukey's multiple comparisons: *P < 0.05. All data are presented as mean ± SEM. (C) Protein expression of OTUB2 and P-ERK in AGS cells infected with *H. pylori* 60190 or ΔCagA. (D) Immunofluorescence images of OTUB2 and CagA in AGS cells infected with *H. pylori* 60190 or ΔCagA for 5 h. Scale bar = 50 μm. (E) AGS cells were transfected with a plasmid-encoding ubiquitin (Ub); 24 h after transfection, the cells were infected with *H. pylori*. YAP ubiquitination was measured by immunoprecipitation. (F) SUMOylation analysis of total lysates and anti-OTUB2 immunoprecipitates from *H. pylori*-infected AGS cells. (G) Fluorescence expression of YAP, CDX2, and ZO-1 in AGS cells treated with rOTUB2 (16 μg/mL). Scale bar = 50 μm. (H) YAP expression in AGS cells infected with *H. pylori* (60190 or ΔCagA) for 5 h after transfection with siOTUB2 for 24 h. (I) Dot plot showing OTUB2 expression according to gastric lesion cell types (the color indicates expression intensity, and the dot size represents the total amount of each cell type). (J) Immunohistochemical images of OTUB2 in human tissues (CSG, IM, IGC, and DGC). Scale bar = 100 μm. (K) Schematic representation of the mechanism by which *H. pylori* CagA-mediated YAP signaling activation promotes metaplasia and early gastric cancer.

6. YAP expression in *H. pylori*-infected human-derived gastric organoids alters the apical junction complex

To investigate the interaction between *H. pylori* and the human gastric epithelial surface, *in vitro H. pylori* infection was modeled in two-dimensional (2D) gastric organoids (Figure 5A).[32] The results revealed that 2D organoids were relatively long-lived, with polarized

epithelial monolayers, and they fully recapitulated various gastric cell lineages. In electron microscopy images, the epithelial surface infected with *H. pylori* 60190 produced mucus (Figure 5B and Supplementary Figure 7D), and the intercellular junctions of the *H. pylori*-infected 2D organoids widened, whereas those of the uninfected 2D organoids remained relatively intact (Figure 5C). The introduction of *H. pylori* 60190 into the mucosa decreased ZO-1 expression, leading to the disruption of the cell monolayer (Figure 5D), and the electrical resistance of the epithelial cells also decreased (Figure 5E). Furthermore, *H. pylori* 60190 strongly induced YAP nuclear expression (Figure 5F), YAP mRNA expression (Figure 5G), and IL-8 production (Figure 5I), as well as a decrease in E-cadherin and PGC expression and an increase in Snail and Muc2 expression (Figure 5H). Single cells isolated from three-dimensional (3D) gastric organoids were transfected with YAP siRNA and YAP overexpression vectors by electroporation and then recultured into 3D organoids. YAP deficiency prevented the formation of 3D organoids, and the YAP-overexpressing organoids exhibited a phenotype similar to that of gastric organoids derived from IGC, with multilumen and multinuclear layering (Figure 5J and 5K).

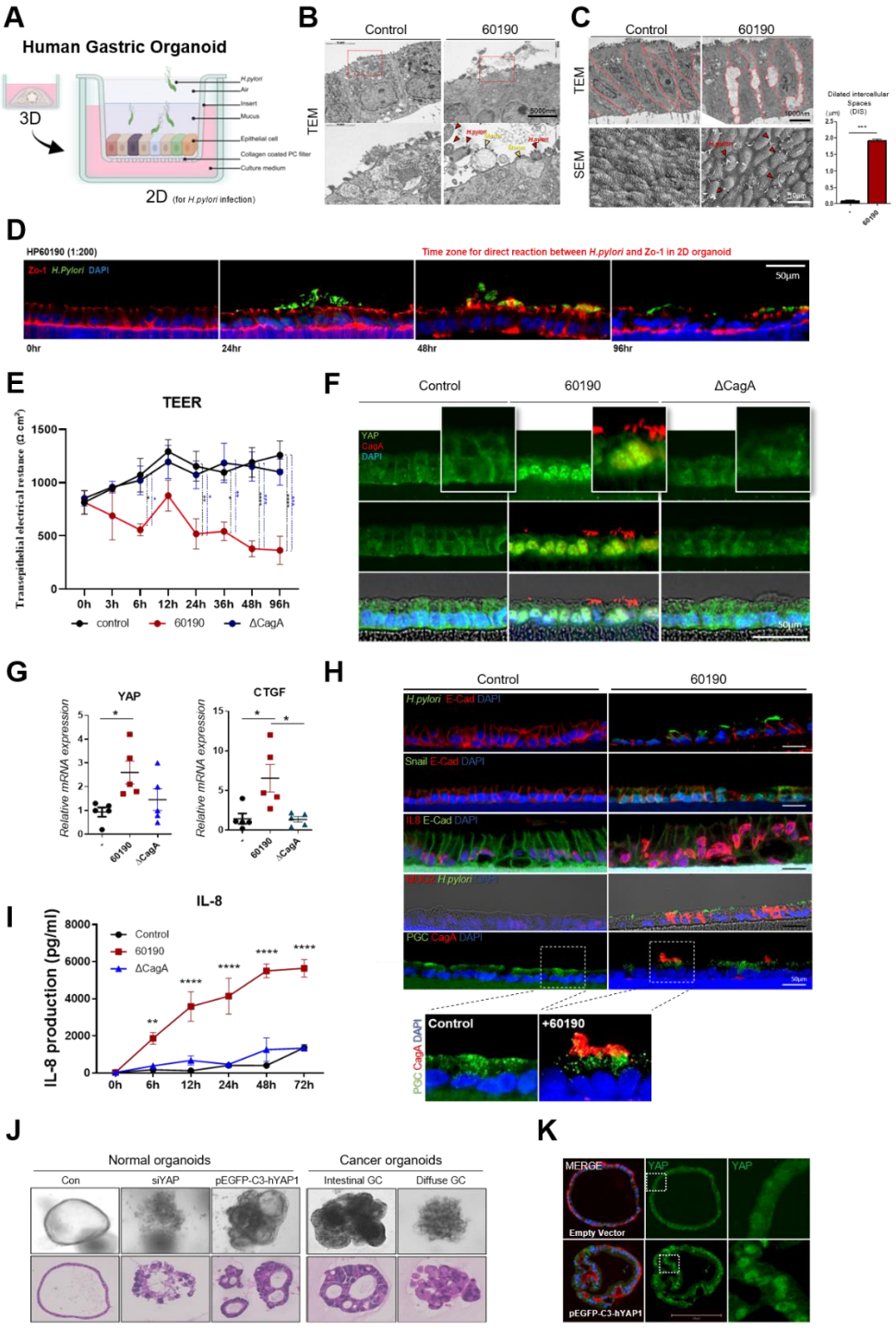

Figure 5. Gastric organoid culture system to mimic actual *in vivo* gastric conditions and chronic inflammatory environments. (A) Schematic of the 2D organoids (mucosoids) culture method: cells are seeded at confluent density onto polycarbonate filters of well inserts placed in a 24-well plate, and the medium above the cell layer is withdrawn after 3 days to initiate air–liquid interface culture. (B) Transmission electron microscopy images of *H. pylori* 60190-infected 2D organoids reveal prominent secretion of mucus, highlighting the morphological changes associated with infection. (C) Transmission electron microscopy (TEM) and scanning electron microscopy (SEM) images of mucosoids treated with control and *H. pylori* 60190 for 48 h. Scale bars: 5000 nm, 1000 nm, and 10 μm (n = 3). (D) Immunofluorescence images of ZO-1 in *H. pylori* 60190-infected 2D organoids. Scale bar = 50 μm. (E) Changes in epithelial electrical resistance values in 2D organoids infected with *H. pylori* 60190 and ΔCagA (n = 4). Statistical analysis was performed using two-way analysis of variance with Tukey's multiple comparisons: *P < 0.05; **P < 0.01; ***P < 0.001; ****P < 0.0001. (F) Immunofluorescence images of YAP and CagA in mucosoids infected with *H. pylori* 60190 and ΔCagA for 48 h. (G) qRT-PCR analysis showing the relative mRNA levels of YAP and connective tissue growth factor in *H. pylori* 60190-infected mucosoids for 48 h. (n = 5). Statistical analysis was performed using one-way analysis of variance with Tukey's multiple comparisons: *P < 0.05. (H) Fluorescent staining images showing changes in the expression levels of E-cadherin, Snail, human IL-8, Muc2, and PGC in *H. pylori* 60190-infected 2D organoids. Scale bar = 50 μm. (I) Human IL-8 production in 2D organoids with and without *H. pylori* infection (n = 5). Statistical analysis was performed using two-way analysis of variance with Tukey's multiple comparisons: **P < 0.01; ****P < 0.0001. (J) Representative images of gastric organoid transfection by electroporation. (K) YAP overexpression using the pEGFP-C3-hYAP1 plasmid vector induced organoid tumorigenesis and YAP nuclear translocation. Scale bar = 250 μm. All data are presented as means ± SEM.

7. YAP/TAZ-knockout gastric chief cells suppress SPEM progression induced by *H. felis* infection

SPEM, which is considered a potential IM precursor, is closely associated with the early stages of gastric carcinogenesis.[37] Gastric chief cells are believed to be the origin of SPEM, and *Helicobacter* infection induces the transdifferentiation of mature chief cells along with inflammatory responses.[10,38-40] To confirm whether chief cells are the origin of YAP/TAZ-mediated SPEM in *H. felis* infection, Mist1-creERT2 $^{Cre/+}$; YAP $^{fl/fl}$; TAZ $^{fl/fl}$ conditional knockout mice and YAP $^{fl/fl}$; TAZ $^{fl/fl}$ control mice were generated (Figure 6A). Previously known *H. pylori* mouse models have highly irregular adaptation to the mouse gastric mucosa and have varied degrees of colonization.[28,41] Therefore, in this study, the highly reproducible *H. felis* mouse model was used to induce lesions similar to human tissue changes (Figure 6B). Stomach samples of *H. felis*-infected YAP/TAZ $^{fl/fl}$ control mice showed strong inflammation, whereas the stomach samples of Mist1-creERT2 $^{Cre/+}$; YAP / TAZ $^{fl/fl}$ conditional knockout mice showed a reduced inflammatory response (Figure 6C). The loss of gastric acid-secreting parietal cells is a well-known representative metaplasia phenotype and is considered an early event in gastric carcinogensis.[42] Therefore, whether YAP/TAZ knockout suppressed metaplasia development in the stomach samples of *H. felis*-infected mice was investigated. *H. felis* infection for 8 weeks caused a significant loss of H^+/K^+-ATPase parietal cells in YAP/TAZ $^{fl/fl}$ control mice but little loss in Mist1-creERT2 $^{Cre/+}$; YAP/TAZ $^{fl/fl}$ knockout mice (Figure 6D). Immunofluorescence images of *H. felis*-infected mice showed that CD44v9 $^{+}$ and GSII $^{+}$/GIF $^{+}$ cells, SPEM markers, were significantly increased in the gland base region. In contrast, the expression of CD44v9 $^{+}$cells and co-expression of GSII $^{+}$/GIF $^{+}$ cells were significantly reduced in Mist1-creERT2 $^{Cre/+}$; YAP/TAZ $^{fl/fl}$ knockout mice (Figure 6E and 6H). In *H. felis*-infected control mice, YAP $^{+}$cells were significantly increased from the base of the gland to the pit, with increased expression primarily in the nucleus. However, in YAP/TAZ-knockout mice, YAP expression was suppressed, and normal morphology of chief cells was preserved without GIF loss (Figure 6F). Levels of Ki-67-proliferating cells were

significantly increased in the upper neck and middle regions of the gastric pit in *H. felis*-infected control mice, whereas no increase in Ki67 cells was observed in the knockout mice (Figure 6G). In control mice infected with *H. felis* for 8 weeks, OTUB2 and SUMO2/3 were mainly expressed in the gastric pit area, where metaplastic changes occurred (Supplementary Figure 8F–8G). Furthermore, *H. felis* infection induced an increase in the number of TFF2-expressing cells and a loss of Mist1 and PGC in mature chief cells. However, YAP/TAZ-knockout mice showed a protective effect against metaplasia-induced changes (Supplementary Figure 8A–8E).

This study demonstrated that YAP/TAZ plays a crucial role in SPEM development induced by *H. felis* infection. The suppression of YAP/TAZ signaling in chief cells prevented the loss of parietal cells and other metaplastic changes. Notably, YAP single knockout showed a less pronounced protective effect compared with a double knockout, highlighting the compensatory role of TAZ in the absence of YAP (Supplementary Figure 9A–9B). These findings propose that YAP/TAZ signaling is a key regulator of *Helicobacter*-induced gastric metaplasia and may contribute to the early events in gastric carcinogenesis (Figure 6I).

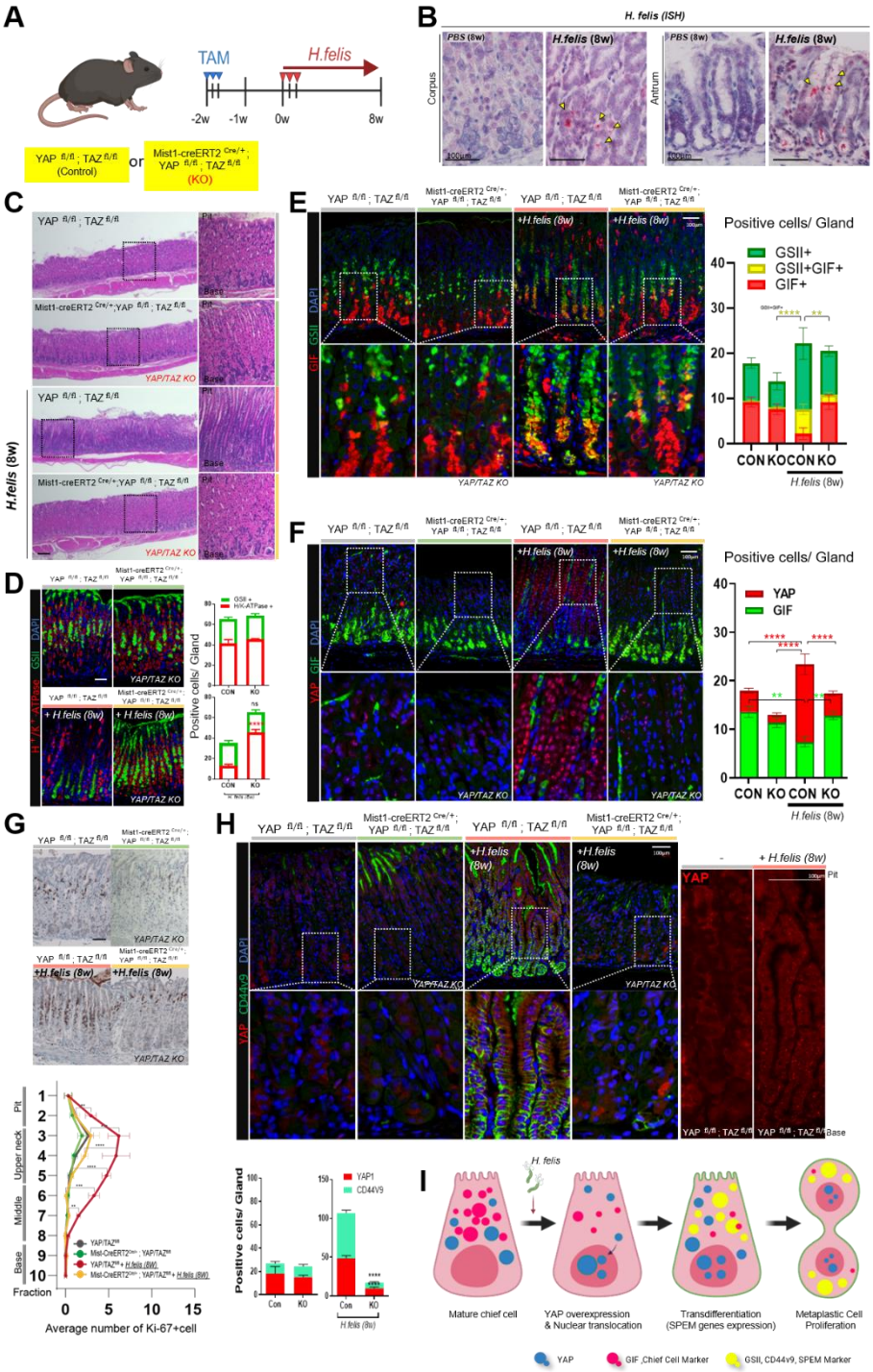

Figure 6. Inhibition of *H. felis*-mediated spasmolytic polypeptide-expressing metaplasia (SPEM) in mice with YAP/TAZ-knockout chief cells. (A) Schematic images showing *H. felis* infection in YAP $^{fl/fl}$; TAZ $^{fl/fl}$ (control) or Mist1-creERT2 $^{Cre/+}$; YAP $^{fl/fl}$; TAZ $^{fl/fl}$ knockout mice.YAP/TAZ was inducibly deleted in mice using the tamoxifen/Cre-loxP system. (B) In situ hybridization images of the *H. felis* probe in mice. (C) Representative H&E staining images of the stomach samples of YAP /TAZ $^{fl/fl}$ (control) / Mist1-creERT2 $^{Cre/+}$; YAP /TAZ $^{fl/fl}$ conditional knockout mice infected with *H. felis*. Scale bar = 100 μm. (D) Immunofluorescence staining of parietal cells (H^+/K^+-ATPase), Griffonia simplicifolia lectin II (GSII), and DAPI in the stomach samples of mice from each group. Quantification of H^+/K^+-ATPase and GSII in single glands (n = 5 per group). Scale bar = 100 μm. (E) Immunofluorescence staining of GSII, gastric intrinsic factor (GIF), and DAPI in the stomach samples of mice in each group. Quantification of GSII $^+$/GIF $^+$ cells per gland (n = 5 per group). Scale bar = 100 μm. (F) Immunofluorescence staining of YAP and GIF in the stomach samples of mice from each group. Quantification of YAP and GIF in single glands (n = 5 per group). Scale bar = 100 μm. (G) Immunohistochemistry for Ki-67 in the mouse stomach samples of each group. To quantify Ki-67 $^+$cells, stomach mucosal tissues were subdivided into 10 fractions (from base to pit region), and Ki-67 $^+$cells were calculated for each fraction (n = 5 per group). Scale bar = 100 μm. (H) Immunofluorescence staining of YAP and CD44v9 in the stomach samples of mice from each group. Quantification of YAP- and CD44v9 $^+$cells in single glands (n = 5 per group). Scale bar = 100 μm. Scale bar = 100 μm. Statistical analysis was performed using two-way analysis of variance with Tukey's multiple comparisons and two-tailed unpaired Student's t-test: *P < 0.05, **P < 0.01, ***P < 0.001, ****P < 0.0001. All data are presented as means ± SEM. (I) Schematic representation of the chief cell transdifferentiation induced by *H. felis*-mediated YAP activation.

8. Exacerbation of SPEM in WT mice by recombinant OTUB2 (rOTUB2) infusion

The effects of exogenous rOTUB2 administration on SPEM development in WT mice were investigated. Fundic samples from WT mice that received rOTUB2 (2 μg/100 μL) showed increased SPEM signatures, enhanced GSII expression, and high YAP expression near the neck cells. Notably, SPEM was induced after 8 weeks of rOTUB2 injection, even in the absence of *H. felis* infection, with a significant increase in oxyntic atrophy (indicated by parietal cell loss) and neck cell accumulation (Figure 7B and 7C). Additionally, the OTUB2 inhibitor (LN5P45) alone effectively suppressed *H. felis*-mediated SPEM. Pretreatment with the OTUB2 inhibitor (2.5 mg/100 μL) prevented both the loss of parietal cells and proliferation of metaplastic cells in *H. felis*-infected mice. Furthermore, in *H. felis*-infected mice treated with the OTUB2 inhibitor, YAP expression was significantly reduced in the neck cells and base region, inhibiting the development of the metaplastic phenotype (Figure 7E and 7F). These findings support the hypothesis that the OTUB2-mediated regulation of YAP expression promotes metaplasia in gastric epithelial cells.

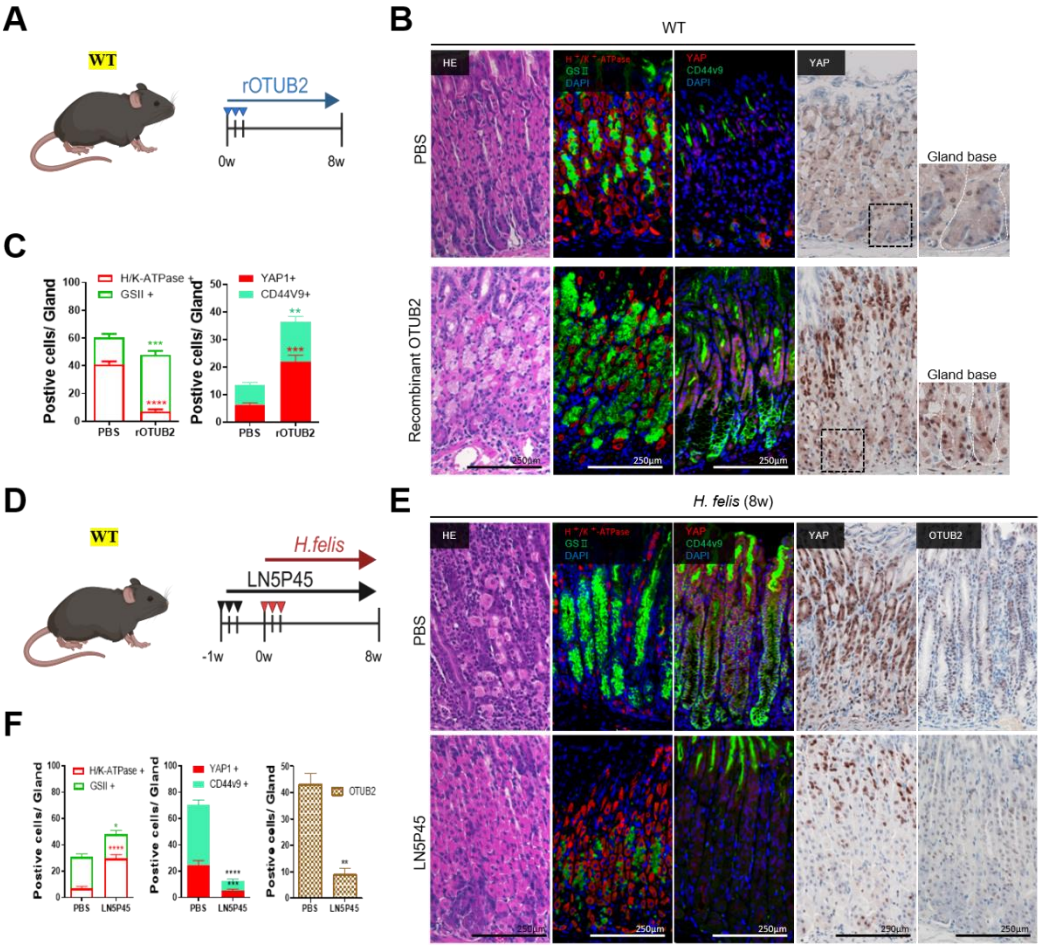

Figure 7. Exacerbation of spasmolytic polypeptide-expressing metaplasia (SPEM) in wild-type mice by rOTUB2 infusion.

(A) Schematic images showing the *in vivo* treatment with recombinant OTUB2 protein. To deliver OTUB2 *in vivo*, recombinant OTUB2 (rOTUB2) was dissolved in PBS and injected intraperitoneally (2 μg/100 μL) every other day for 7 days. (B) Representative immunohistochemical images for SPEM markers (CD44v9), parietal cells (H^+/K^+-ATPase), GSII, and YAP in wild-type mice injected with rOTUB2. Scale bar = 250 μm. (C) Comparison of positive cells in rOTUB2-injected mice. Each graph represents the number

of positive cells in a single sample (n = 5 per group). (D) Schematic images showing *in vivo* treatment with OTUB2 inhibitor (LN5P45) and *H. felis* infection method. OTUB2 inhibitor (LN5P45, 2.5mg/100 μL) was injected intraperitoneally into wild-type mice, followed by *H. felis* infection. (E) Representative immunohistochemical images for CD44v9, H^+/K^+-ATPase, GSII, YAP, and OTUB2 in wild-type mice pretreated with LN5P45 and infected with *H. felis*. Scale bar = 250 μm. (F) Comparison of positive cells in LN5P45-pretreated mice infected with *H. felis*. Each graph represents the number of positive cells per single gland (n = 5 per group). Two-tailed unpaired Student's t-test: *P < 0.05; **P < 0.01; ***P < 0.001; ****P < 0.0001. All data are presented as means ± SEM.

IV. DISCUSSION

Previous studies have explored Hippo signaling pathway genes as candidate biomarkers for various types of human cancer. Patients with high expression of Hippo signaling pathway genes such as YAP/TAZ generally have poor prognoses.[12,13] In this study, YAP expression was higher than that of TAZ and was overexpressed in metaplasia and gastric cancer, confirming the central role of YAP in the development and progression of gastric cancer. Despite the effects of YAP on numerous diseases, the molecular mechanism of YAP in *Helicobacter*-mediated gastric carcinogenesis remains unclear. In this study, cellular YAP levels were increased by CagA-positive *H. pylori* in human gastric epithelial cells, and expression levels of CDX2 (an IM marker) were higher. GSEA data showed upregulation of several gene sets associated with inflammation, YAP signaling, K63-linked deubiquitination, and gastric carcinogenesis in *H. pylori*-infected gastric epithelial cells. In particular, *H. pylori* 60190 (CagA-positive) infection leads to the activation of an inflammatory signaling pathway that induces proinflammatory cytokines such as IL-8.[3] *H. pylori* infection induces chronic inflammation in the gastric mucosa, leading to metaplastic changes such as SPEM and IM, which are precursors to gastric cancer.[5]

Previously, we reported that *H. pylori* CagA acts as a pathogenic scaffold protein that induces snail-mediated epithelial–mesenchymal transition through GSK-3 depletion.[43] In this study, *H. pylori* 60190 altered the structure of the apical junction by downregulating the scaffolding protein ZO-1 through YAP overexpression in gastric cancer. YAP and ZO-1 colocalize at the plasma membrane to form tight junction scaffolds.[23,44,45] *H. pylori* infection leads to the downregulation of the ZO-1 protein, widening of intercellular junctions, and increased permeability through YAP overexpression. This change stimulates cell proliferation and migration and may promote cancer progression. This finding suggests that YAP inhibits the synthesis of ZO-1 mRNAs and proteins through downstream signaling factors such as TEAD and CTGF and transcription factors such as Snail and Slug.[46,47] In this study, YAP-knockout cells can reverse *Helicobacter*-mediated ZO-1 downregulation, providing evidence that YAP expression influences ZO-1 relocalization and

downregulation.[48-50] Moreover, 2D gastric organoids that recapitulate the physiological function and tissue characteristics of the human stomach mucosa were infected with *H. pylori*. *H. pylori* passing through the gastric mucus induced the loss of epithelial cell morphology, decreased the expression of proteins mediating cell–cell contact, remodeled the actin cytoskeleton system, and acquired a mesenchymal cell morphology. 2D organoid cultures are suitable for investigating early carcinogenetic events because they mimic *in vivo* gastric conditions and can extend the infection period and chronic inflammatory environment.[32] Induced YAP expression in 3D normal gastric organoids resulted in an organoid phenotype similar to that of gastric organoids derived from intestinal-type gastric cancer. However, YAP deficiency limited organoid formation, leading to gastric organoid growth failure. This finding indicates the importance of YAP in tissue formation and growth in the human stomach and maintenance of an appropriate balance of intracellular YAP.

In this study, a set of lysine 63 (K63)-linked DUB genes that were upregulated in *H. pylori*-infected cell lines was identified, and OTUB2 was found to interact with YAP to induce YAP deubiquitination, contributing to the activation of YAP-dependent gene expression. OTUB2 was an important regulator of YAP signaling in *H. pylori*-mediated gastric carcinogenesis. Furthermore, in human gastric tissues, OTUB2 RNA expression levels were the highest in IM cells, signifying that OTUB2 contributes to gastric cancer development by activating YAP at the precancerous IM stage. Previous studies have demonstrated that *H. felis* causes a more severe gastric disease in mice than does *H. pylori*.[28,41] SPEM induction through *H. felis* infection generates oxyntic atrophy and causes abnormal gland morphology. In this study, knockout mice, in which YAP/TAZ is suppressed in the chief cells, were used to demonstrate YAP/TAZ involvement in the development of epithelial metaplasia and the transdifferentiation of the chief cells. These metaplastic cells express a distinct molecular signature, including the coexpression of GSII and GIF, intestinal transcriptome, and CD44v9.[38,39] Metaplastic changes in the gastric epithelium not only alter cellular morphology but also reprogram gene expression patterns, resulting in a cellular environment conducive to further carcinogenesis. The transformation

of chief cells into SPEM cells and the subsequent downregulation of gastric differentiation markers, together with the upregulation of intestinal-like markers, may drive the progression toward gastric cancer. Our findings demonstrate the downregulation of genes associated with SPEM and gastric cancer in *H. felis*-infected mice with YAP/TAZ knockout in the gastric chief cells. Therefore, YAP/TAZ may play an important role in the transdifferentiation of gastric chief cells into SPEM cells. Furthermore, this mechanism is regulated by the deubiquitination enzyme OTUB2 through the inhibition of YAP degradation. Taken together, these results emphasize the role of YAP in *Helicobacter*-mediated gastric carcinogenesis and demonstrate that OTUB2-upregulated YAP promotes premalignant metaplasia and gastric carcinogenesis by inducing the remodeling of the actin cytoskeleton and the transdifferentiation of gastric epithelial cells.

In conclusion, this study comprehensively demonstrated the crucial role of YAP in the development and progression of *Helicobacter*-mediated gastric cancer and that OTUB2 may serve as a novel regulator of YAP signaling. Notably, YAP also plays an important role in SPEM and IM development, which serve as a precursor to gastric cancer and may further promote carcinogenesis. These findings provide new insights into the role of YAP in *Helicobacter*-induced gastric cancer development and progression and shed light on the link between metaplasia and cancer initiation.

V. CONCLUSION

YAP plays a central role in epithelial transformation leading to gastric cancer in *Helicobacter*-mediated gastric cancer. In addition, nuclear translocation of YAP acts together with coactivators such as TEAD, playing a key role in metaplasia formation and gastric carcinogenesis. Nuclear translocation of YAP not only contributes to EMT by weakening binding proteins such as ZO-1, but induces metaplastic transformation through overexpression of CDX2. In addition, *H. pylori*–mediated YAP overexpression is associated with the production of the proinflammatory cytokine IL-8, and *H. pylori* CagA

plays a key role in YAP nuclear translocation. Significant changes were observed in patient-derived gastric organoids that have physiological activities similar to those in human gastric mucosa. YAP deficiency suppressed *H. pylori*–mediated epithelial transformation and disrupted the formation of gastric organoids. We also identified a novel YAP activation mechanism in addition to the canonical Hippo signaling. We found that the deubiquitinating enzyme OTUB2 prevents YAP degradation through deubiquitination and contributes to metaplastic change and gastric carcinogenesis. OTUB2 binds to YAP and increases its activation stability. These results suggest that YAP/TAZ deficiency alone suppresses histological changes and the generation of spasmolytic polypeptide-expressing metaplasia (SPEM) phenotypes in chief cells of mice infected with *H. felis*. Injection of rOTUB2 induced neck-cell hyperplasia and SPEM phenotype generation in wild-type mice. In summary, we have comprehensively shown that YAP plays an important role in the development and progression of *Helicobacter*-mediated gastric carcinogenesis, and that OTUB2 may serve as a novel regulator of YAP signal regulation. These findings provide new insights into the role of YAP/TAZ in *Helicobacter*-mediated gastric cancer development and progression.

References

1. Xu E, Xia X, Jiang C, Li Z, Yang Z, Zheng C, et al. GPER1 Silencing Suppresses the Proliferation, Migration, and Invasion of Gastric Cancer Cells by Inhibiting PI3K/AKT-Mediated EMT. Front Cell Dev Biol 2020;8:591239.
2. Morgan E, Arnold M, Camargo MC, Gini A, Kunzmann AT, Matsuda T, et al. The current and future incidence and mortality of gastric cancer in 185 countries, 2020-40: A population-based modelling study. EClinicalMedicine 2022;47:101404.
3. Fazeli Z, Alebouyeh M, Rezaei Tavirani M, Azimirad M, Yadegar A. Helicobacter pylori CagA induced interleukin-8 secretion in gastric epithelial cells. Gastroenterol Hepatol Bed Bench 2016;9:S42-S6.
4. Kim BJ. Natural Course of Atrophic Gastritis and Intestinal Metaplasia. The Korean Journal of Helicobacter and Upper Gastrointestinal Research 2020;20:101-6.
5. Li ML, Hong XX, Zhang WJ, Liang YZ, Cai TT, Xu YF, et al. Helicobacter pylori plays a key role in gastric adenocarcinoma induced by spasmolytic polypeptide-expressing metaplasia. World J Clin Cases 2023;11:3714-24.
6. Liu Q, Teh M, Ito K, Shah N, Ito Y, Yeoh KG. CDX2 expression is progressively decreased in human gastric intestinal metaplasia, dysplasia and cancer. Mod Pathol 2007;20:1286-97.
7. Qin R, Wang NN, Chu J, Wang X. Expression and significance of homeodomain protein Cdx2 in gastric carcinoma and precancerous lesions. World J Gastroenterol 2012;18:3296-302.
8. Lee BH, Kim N, Lee HS, Kang JM, Park HK, Jo HJ, et al. The Role of CDX2 in Intestinal Metaplasia Evaluated Using Immunohistochemistry. Gut Liver 2012;6:71-7.
9. Goldenring JR, Mills JC. Cellular Plasticity, Reprogramming, and Regeneration: Metaplasia in the Stomach and Beyond. Gastroenterology 2022;162:415-30.
10. Caldwell B, Meyer AR, Weis JA, Engevik AC, Choi E. Chief cell plasticity is the

origin of metaplasia following acute injury in the stomach mucosa. Gut 2022;71:1068-77.

11. Hirata K, Suzuki H, Imaeda H, Matsuzaki J, Tsugawa H, Nagano O, et al. CD44 variant 9 expression in primary early gastric cancer as a predictive marker for recurrence. Br J Cancer 2013;109:379-86.
12. Loe AKH, Rao-Bhatia A, Wei Z, Kim JE, Guan B, Qin Y, et al. YAP targetome reveals activation of SPEM in gastric pre-neoplastic progression and regeneration. Cell Rep 2023;42:113497.
13. Ma S, Meng Z, Chen R, Guan KL. The Hippo Pathway: Biology and Pathophysiology. Annu Rev Biochem 2019;88:577-604.
14. Mokhtari RB, Ashayeri N, Baghaie L, Sambi M, Satari K, Baluch N, et al. The Hippo Pathway Effectors YAP/TAZ-TEAD Oncoproteins as Emerging Therapeutic Targets in the Tumor Microenvironment. Cancers (Basel) 2023;15.
15. Messina B, Lo Sardo F, Scalera S, Memeo L, Colarossi C, Mare M, et al. Hippo pathway dysregulation in gastric cancer: from Helicobacter pylori infection to tumor promotion and progression. Cell Death Dis 2023;14:21.
16. Yao F, Zhou Z, Kim J, Hang Q, Xiao Z, Ton BN, et al. SKP2- and OTUD1-regulated non-proteolytic ubiquitination of YAP promotes YAP nuclear localization and activity. Nat Commun 2018;9:2269.
17. Zhang Z, Du J, Wang S, Shao L, Jin K, Li F, et al. OTUB2 Promotes Cancer Metastasis via Hippo-Independent Activation of YAP and TAZ. Mol Cell 2019;73:7-21 e7.
18. Qian M, Yan F, Wang W, Du J, Yuan T, Wu R, et al. Deubiquitinase JOSD2 stabilizes YAP/TAZ to promote cholangiocarcinoma progression. Acta Pharm Sin B 2021;11:4008-19.
19. Manohar S, Jacob S, Wang J, Wiechecki KA, Koh HWL, Simoes V, et al. Polyubiquitin Chains Linked by Lysine Residue 48 (K48) Selectively Target Oxidized Proteins In Vivo. Antioxid Redox Signal 2019;31:1133-49.

20. Altun M, Walter TS, Kramer HB, Herr P, Iphofer A, Bostrom J, et al. The human otubain2-ubiquitin structure provides insights into the cleavage specificity of poly-ubiquitin-linkages. PLoS One 2015;10:e0115344.
21. Zihni C, Mills C, Matter K, Balda MS. Tight junctions: from simple barriers to multifunctional molecular gates. Nat Rev Mol Cell Biol 2016;17:564-80.
22. Tornavaca O, Chia M, Dufton N, Almagro LO, Conway DE, Randi AM, et al. ZO-1 controls endothelial adherens junctions, cell-cell tension, angiogenesis, and barrier formation. J Cell Biol 2015;208:821-38.
23. Kim SY, Park SY, Jang HS, Park YD, Kee SH. Yes-Associated Protein Is Required for ZO-1-Mediated Tight-Junction Integrity and Cell Migration in E-Cadherin-Restored AGS Gastric Cancer Cells. Biomedicines 2021;9.
24. Kuo WT, Zuo L, Odenwald MA, Madha S, Singh G, Gurniak CB, et al. The Tight Junction Protein ZO-1 Is Dispensable for Barrier Function but Critical for Effective Mucosal Repair. Gastroenterology 2021;161:1924-39.
25. Yoshida K, Kanaoka S, Takai T, Uezato T, Miura N, Kajimura M, et al. EGF rapidly translocates tight junction proteins from the cytoplasm to the cell-cell contact via protein kinase C activation in TMK-1 gastric cancer cells. Exp Cell Res 2005;309:397-409.
26. Huo L, Wen W, Wang R, Kam C, Xia J, Feng W, et al. Cdc42-dependent formation of the ZO-1/MRCKbeta complex at the leading edge controls cell migration. EMBO J 2011;30:665-78.
27. Yu S, He J, Xie K. Zonula Occludens Proteins Signaling in Inflammation and Tumorigenesis. Int J Biol Sci 2023;19:3804-15.
28. Druffner SR, Venkateshwaraprabu S, Khadka S, Duncan BC, Morris MT, Sen-Kilic E, et al. Comparison of gastric inflammation and metaplasia induced by Helicobacter pylori or Helicobacter felis colonization in mice. bioRxiv 2023; doi:10.1101/2023.12.22.573128.
29. Mohammadi M, Redline R, Nedrud J, Czinn S. Role of the host in pathogenesis of

Helicobacter-associated gastritis: H. felis infection of inbred and congenic mouse strains. Infect Immun 1996;64:238-45.

30. Kim J, Park C, Kim KH, Kim EH, Kim H, Woo JK, et al. Single-cell analysis of gastric pre-cancerous and cancer lesions reveals cell lineage diversity and intratumoral heterogeneity. NPJ Precis Oncol 2022;6:9.
31. Bartfeld S, Bayram T, van de Wetering M, Huch M, Begthel H, Kujala P, et al. In vitro expansion of human gastric epithelial stem cells and their responses to bacterial infection. Gastroenterology 2015;148:126-36 e6.
32. Boccellato F, Woelffling S, Imai-Matsushima A, Sanchez G, Goosmann C, Schmid M, et al. Polarised epithelial monolayers of the gastric mucosa reveal insights into mucosal homeostasis and defence against infection. Gut 2019;68:400-13.
33. Fang J, Jadhav PR. From in vitro EC(5)(0) to in vivo dose-response for antiretrovirals using an HIV disease model. Part II: application to drug development. J Pharmacokinet Pharmacodyn 2012;39:369-81.
34. van Soldt BJ, Cardoso WV. Hippo-Yap/Taz signaling: Complex network interactions and impact in epithelial cell behavior. Wiley Interdiscip Rev Dev Biol 2020;9:e371.
35. Goswami S, Balasubramanian I, D'Agostino L, Bandyopadhyay S, Patel R, Avasthi S, et al. RAB11A-mediated YAP localization to adherens and tight junctions is essential for colonic epithelial integrity. J Biol Chem 2021;297:100848.
36. Eaton KA, Ringler SR, Danon SJ. Murine splenocytes induce severe gastritis and delayed-type hypersensitivity and suppress bacterial colonization in Helicobacter pylori-infected SCID mice. Infect Immun 1999;67:4594-602.
37. Jeong H, Lee B, Kim KH, Cho SY, Cho Y, Park J, et al. WFDC2 Promotes Spasmolytic Polypeptide-Expressing Metaplasia Through the Up-Regulation of IL33 in Response to Injury. Gastroenterology 2021;161:953-67 e15.
38. Nam KT, Lee HJ, Sousa JF, Weis VG, O'Neal RL, Finke PE, et al. Mature chief cells are cryptic progenitors for metaplasia in the stomach. Gastroenterology

2010;139:2028-37 e9.

39. Choi E, Hendley AM, Bailey JM, Leach SD, Goldenring JR. Expression of Activated Ras in Gastric Chief Cells of Mice Leads to the Full Spectrum of Metaplastic Lineage Transitions. Gastroenterology 2016;150:918-30 e13.
40. Weis VG, Petersen CP, Weis JA, Meyer AR, Choi E, Mills JC, et al. Maturity and age influence chief cell ability to transdifferentiate into metaplasia. Am J Physiol Gastrointest Liver Physiol 2017;312:G67-G76.
41. Ng G, Every A, McGuckin M, Sutton P. Increased Helicobacter felis colonization in male 129/Sv mice fails to suppress gastritis. Gut Microbes 2011;2:358-60.
42. Zeller G, Tap J, Voigt AY, Sunagawa S, Kultima JR, Costea PI, et al. Potential of fecal microbiota for early-stage detection of colorectal cancer. Mol Syst Biol 2014;10:766.
43. Lee DG, Kim HS, Lee YS, Kim S, Cha SY, Ota I, et al. Helicobacter pylori CagA promotes Snail-mediated epithelial-mesenchymal transition by reducing GSK-3 activity. Nat Commun 2014;5:4423.
44. Thrash HL, Pendergast AM. Multi-Functional Regulation by YAP/TAZ Signaling Networks in Tumor Progression and Metastasis. Cancers (Basel) 2023;15:4701.
45. Rouaud F, Sluysmans S, Flinois A, Shah J, Vasileva E, Citi S. Scaffolding proteins of vertebrate apical junctions: structure, functions and biophysics. Biochim Biophys Acta Biomembr 2020;1862:183399.
46. Akrida I, Bravou V, Papadaki H. The deadly cross-talk between Hippo pathway and epithelial-mesenchymal transition (EMT) in cancer. Mol Biol Rep 2022;49:10065-76.
47. Kim BJ, Hancock BM, Bermudez A, Del Cid N, Reyes E, van Sorge NM, et al. Bacterial induction of Snail1 contributes to blood-brain barrier disruption. J Clin Invest 2015;125:2473-83.
48. Huang Z, Zhang Z, Zhou C, Liu L, Huang C. Epithelial-mesenchymal transition: The history, regulatory mechanism, and cancer therapeutic opportunities.

MedComm (2020) 2022;3:e144.

49. Shu DY, Butcher E, Saint-Geniez M. EMT and EndMT: Emerging Roles in Age-Related Macular Degeneration. Int J Mol Sci 2020;21.

50. Ashrafizadeh M, Dai J, Torabian P, Nabavi N, Aref AR, Aljabali AAA, et al. Circular RNAs in EMT-driven metastasis regulation: modulation of cancer cell plasticity, tumorigenesis and therapy resistance. Cell Mol Life Sci 2024;81:214.

APPENDICE

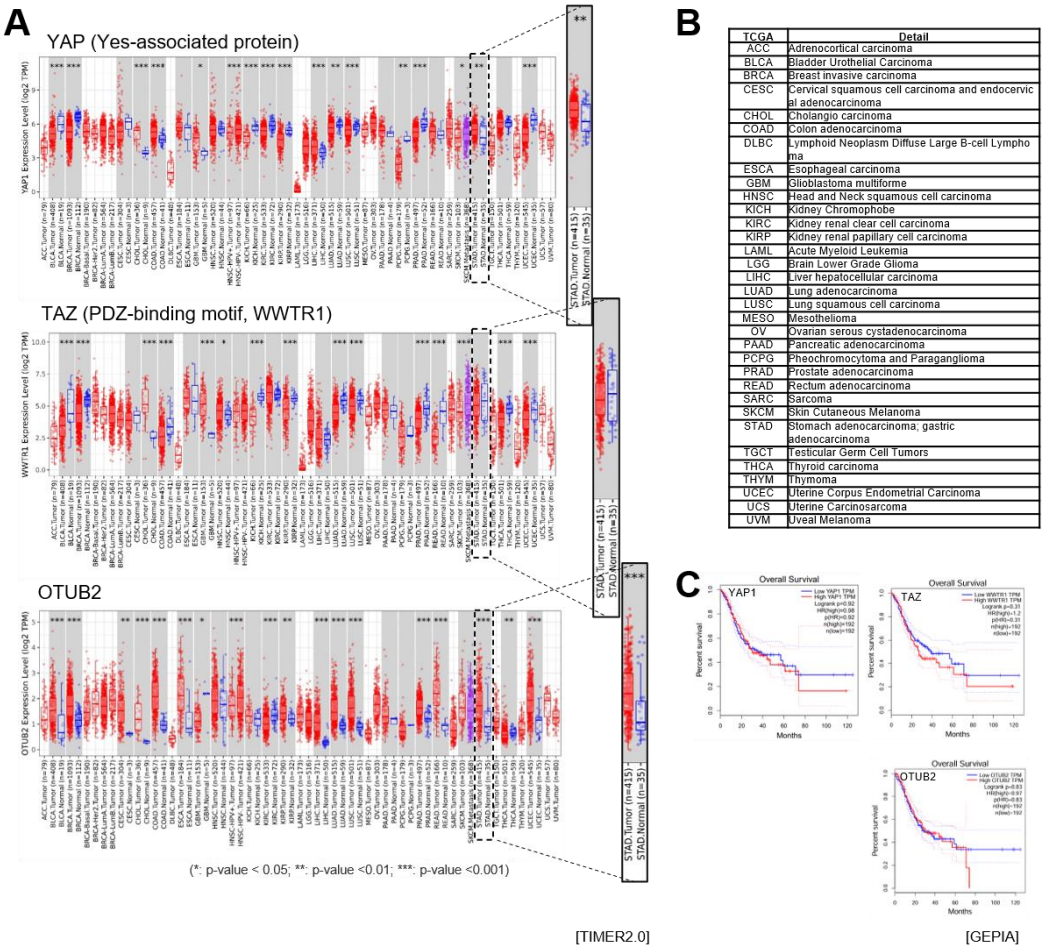

TCGA	Detail
ACC	Adrenocortical carcinoma
BLCA	Bladder Urothelial Carcinoma
BRCA	Breast invasive carcinoma
CESC	Cervical squamous cell carcinoma and endocervical adenocarcinoma
CHOL	Cholangio carcinoma
COAD	Colon adenocarcinoma
DLBC	Lymphoid Neoplasm Diffuse Large B-cell Lymphoma
ESCA	Esophageal carcinoma
GBM	Glioblastoma multiforme
HNSC	Head and Neck squamous cell carcinoma
KICH	Kidney Chromophobe
KIRC	Kidney renal clear cell carcinoma
KIRP	Kidney renal papillary cell carcinoma
LAML	Acute Myeloid Leukemia
LGG	Brain Lower Grade Glioma
LIHC	Liver hepatocellular carcinoma
LUAD	Lung adenocarcinoma
LUSC	Lung squamous cell carcinoma
MESO	Mesothelioma
OV	Ovarian serous cystadenocarcinoma
PAAD	Pancreatic adenocarcinoma
PCPG	Pheochromocytoma and Paraganglioma
PRAD	Prostate adenocarcinoma
READ	Rectum adenocarcinoma
SARC	Sarcoma
SKCM	Skin Cutaneous Melanoma
STAD	Stomach adenocarcinoma; gastric adenocarcinoma
TGCT	Testicular Germ Cell Tumors
THCA	Thyroid carcinoma
THYM	Thymoma
UCEC	Uterine Corpus Endometrial Carcinoma
UCS	Uterine Carcinosarcoma
UVM	Uveal Melanoma

Supplementary Figure 1. YAP, TAZ, and OTUD2 are abnormally expressed in various types of tumors. (A) Analysis of data from the TCGA database showed that YAP and OTUB2 expression was significantly higher in gastric cancer (STAD) than in adjacent normal tissues, while TAZ (WWTR1) did not achieve significant results. Data were analyzed using TIMER2.0 database (http://timer.cistrome.org). Statistical analysis was performed using the Wilcoxon signed-rank test. *P < 0.05, **P < 0.01, ***P < 0.001. (B) Abbreviation of cancer name. (C) Overall survival of YAP, TAZ, and OTUD2 in gastric cancer (STAD). A Kaplan–Meier survival analysis was applied to compare survival rates for patients with gastric adenocarcinoma using a log-rank test.

Supplementary Figure 2. Single-cell analysis of precancerous and cancerous lesions. (A) A t-distributed stochastic neighbor embedding (t-SNE) map for 48,670 single cells filtered from adjacent noncancerous and cancerous tissues. (B) t-SNE plot showing Hippo pathway genes, gastric marker, and IM marker genes in CSG (chronic superficial gastritis,), IM (intestinal type gastric cancer), IGC (intestinal type gastric cancer), and DGC (diffuse type gastric cancer). Colors represent cell types based on expression of known marker genes. (C) Dot plot showing the expression of Hippo pathway genes and OTUB2 according to the gastric lesion cell types (the color indicates expression intensity, and the dot size indicates the total amount of each cell type). CSG, chronic superficial gastritis; DGC, diffuse type gastric cancer; IGC, intestinal type gastric cancer; IM, intestinal metaplasia; GMC, gland mucous cell; PMC, pit mucous cell

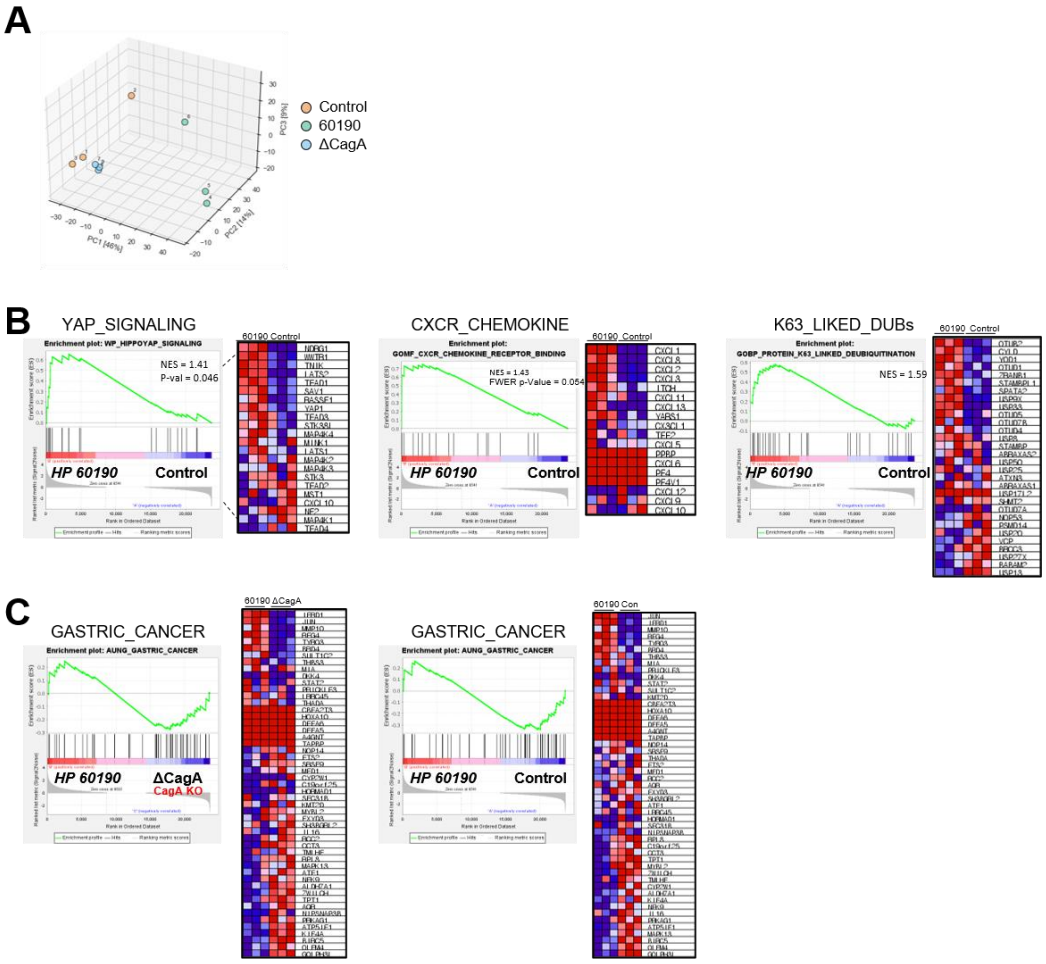

Supplementary Figure 3. Transcriptome analysis of uninfected AGS cells and *H. pylori* (60190, ΔCagA)-infected AGS cells. (A) Principal component analysis (PCA) plot showing the similarity between uninfected AGS cells and *H. pylori* (60190, ΔCagA)-infected AGS cell samples using normalized signals. (B, C) GSEA plots for YAP signaling-related gene sets, CXCR chemokine receptor-binding gene sets, K63-linked deubiquitination gene sets, and gastric cancer-related gene sets comparing uninfected AGS cells and *H. pylori* (60190, ΔCagA)-infected AGS cells.

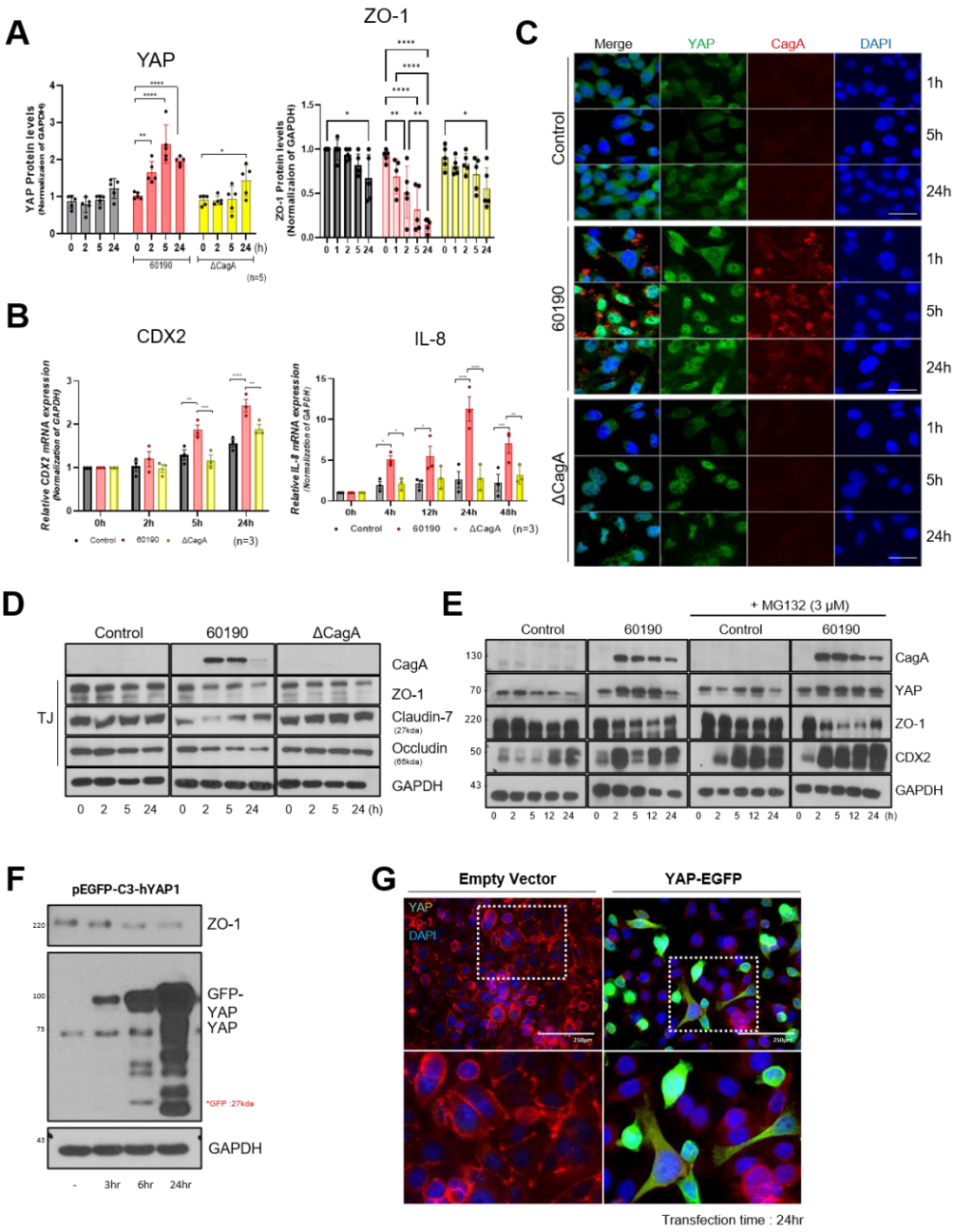

Supplementary Figure 4. Changes in YAP and Tight Junction Protein in AGS Cells Infected with *H. pylori*. (A) Graph showing the fold change in YAP and ZO-1 protein expression in AGS cells infected with *H. pylori* 60190 and ΔCagA over the indicated time periods. (n = 5 per group).

Statistical analysis was performed using two-way analysis of variance with Tukey's multiple comparisons : *P < 0.05; **P < 0.01; ***P < 0.001; ****P < 0.0001. (B) Graph showing the fold change in CDX2 and IL-8 mRNA expression in AGS cells infected with *H. pylori* 60190 and ΔCagA. (n = 3 per group). Statistical analysis was performed using two-way analysis of variance with Tukey's multiple comparisons : *P < 0.05; **P < 0.01; ***P < 0.001; ****P < 0.0001. (C) AGS cells were infected with *H. pylori* 60190 and ΔCagA for the indicated time periods. Cells were then fixed for immunofluorescence staining of YAP and CagA. Scale bar = 50 μm. (D) AGS cells were infected with *H. pylori* (60190, ΔCagA) for the indicated time periods, and the expression of tight-junction proteins (ZO-1, claudin-7, and occludin) was confirmed by western blotting. (E) AGS cells were treated with *H. pylori* 60190 for the indicated time periods in the presence or absence of MG132 (3 μM). The proteasome inhibitor MG132 inhibited the degradation of YAP, leading to its persistent accumulation within the cells, which may further promote the reduction of ZO-1. (F) Western blot data showing the expression of YAP and ZO-1 in AGS cells transfected with pEGFP-C3-hYAP1 (plasmid #17843, Addgene) for up to 24 h. (G) Immunofluorescence images showing the expression of YAP and ZO-1 in AGS cells transfected with pEGFP-C3-hYAP1 (plasmid #17843, Addgene) for up to 24 h. Scale bar = 250 μm.

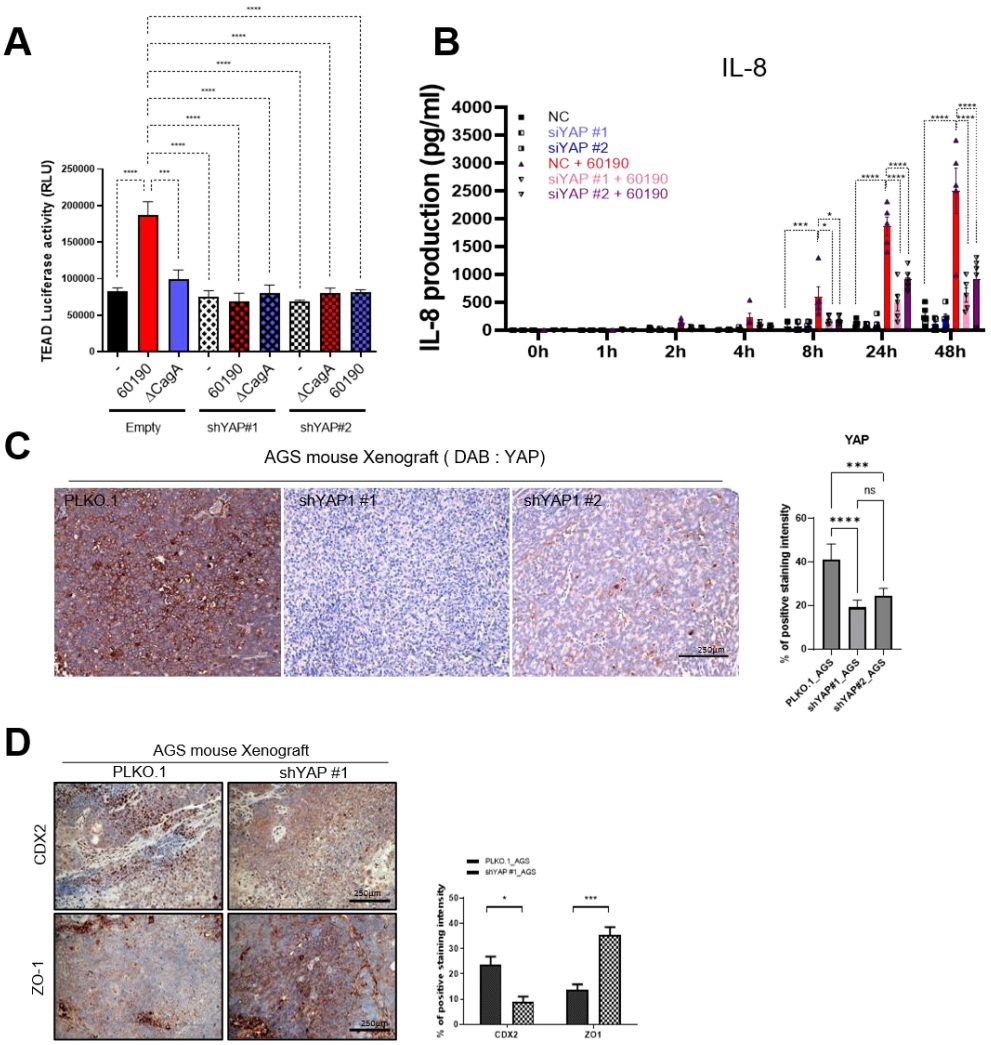

Supplementary Figure 5. DAB Staining Analysis of YAP, ZO-1 and CDX2 in AGS Xenograft Tumors. (A) Luciferase activity of TEAD reporter constructs analyzed during *H. pylori* infection in YAP-silenced AGS cells (PLKO.1, shYAP #1, shYAP #2). YAP-TEAD protein-protein interactions mediate the downstream oncogenic functions of YAP in the Hippo pathway. As the transcriptional coactivator, YAP localizes to the nucleus and induces the expression of TEAD luciferase reporter genes. The TEAD luciferase reporter was activated in *H. pylori* 60190–infected AGS cells, whereas TEAD luciferase activity did not increase in YAP-knockout AGS cells (shYAP #1 and shYAP #2). Statistical analysis was performed using two-way analysis of variance with Tukey's multiple

comparisons: *P < 0.05; **P < 0.01; ***P < 0.001 ; ****P < 0.0001. (B) IL-8 production in siYAP-transfected AGS cells with or without *H. pylori* infection was confirmed by ELISA (n = 5 per group). Downregulation of YAP significantly reduced *H. pylori*–mediated production of IL-8. Statistical analysis was performed using two-way analysis of variance with Tukey's multiple comparisons: *P < 0.05; **P < 0.01; ***P < 0.001 ; ****P < 0.0001. (C) DAB staining of YAP in AGS xenograft tumors (n = 5 per group). Statistical analysis was performed using one-way analysis of variance with Tukey's multiple comparisons: ***P < 0.001 ; ****P < 0.0001. (D) DAB staining of CDX2 and ZO-1 in AGS xenograft tumors. Quantification graph for positive cells in AGS xenograft tumors (n = 3 per group). Statistical analysis was performed using two-tailed unpaired Student's t-test: *P < 0.05; ***P < 0.001.

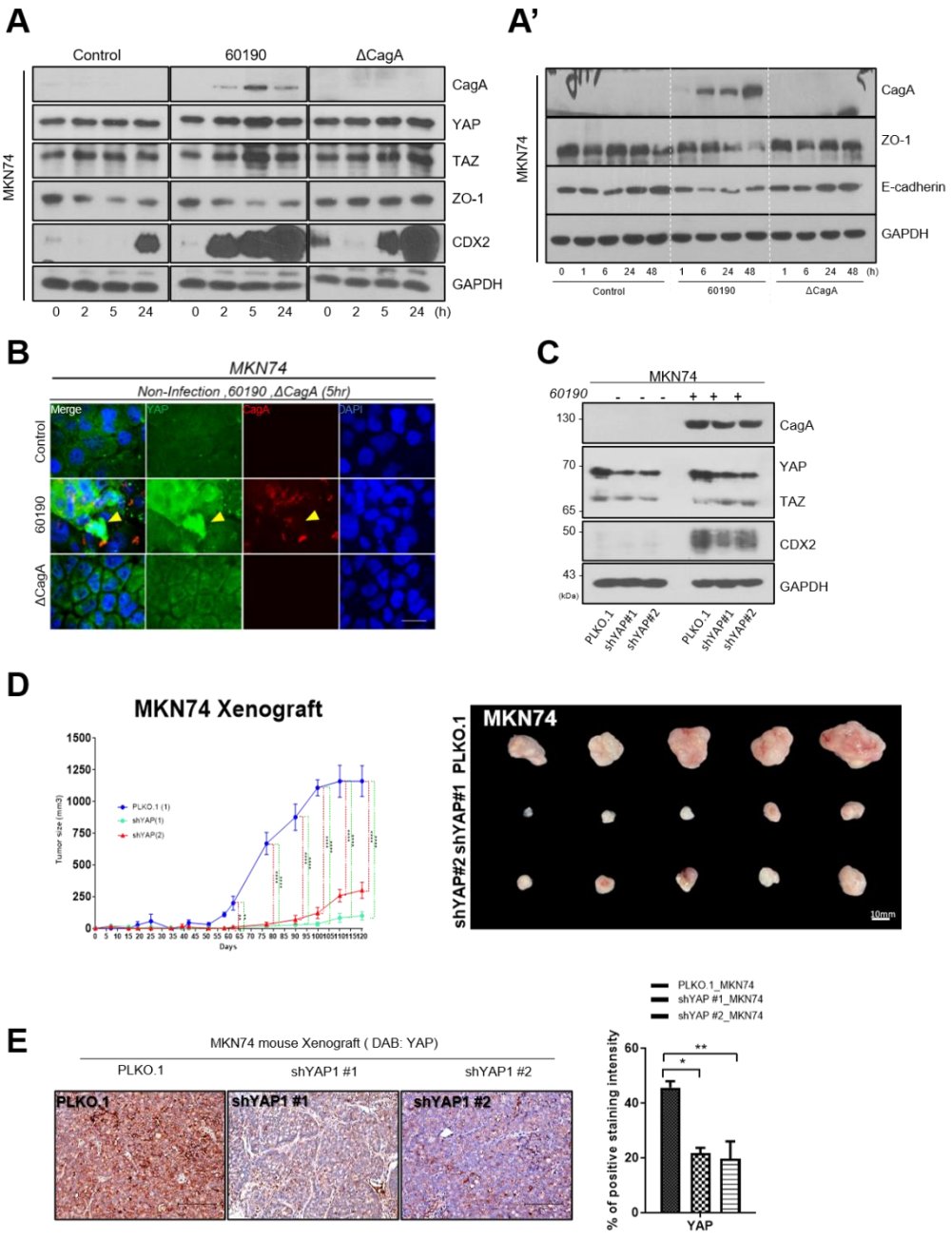

Supplementary Figure 6. YAP expression and Tumor Growth in Response to *H. pylori* Infection in MKN74 cells. (A) MKN74 cells were infected with *H. pylori* 60190 or ΔCagA for the indicated

periods, and YAP/TAZ expression was confirmed by Western blotting of harvested cell lysates. (B) MKN74 cells were infected with *H. pylori* 60190 or ΔCagA for 5 h. Cells were fixed for immunofluorescence staining of YAP and CagA. Scale bar = 50 μm. (C) Western blot analysis was performed to confirm protein expression of CDX2 in YAP-silenced MKN74 cells. (D) Tumor size after subcutaneous injection of mice with MKN74-PLKO.1 or shYAP#1, #2 (n = 5 per group). Statistical analysis was performed using two-way analysis of variance with Tukey's multiple comparisons: *P < 0.05; **P < 0.01; ***P < 0.001; ****P < 0.0001. (E) DAB staining and quantification of YAP-positive cells in MKN74 xenograft tumors (n = 3 per group). Each graph represents the number of positive cells in the transplanted tumors (n = 5 per group). Statistical analysis was performed using one-way analysis of variance with Tukey's multiple comparisons: *P < 0.05; **P < 0.01. All data are presented as means ± SEM.

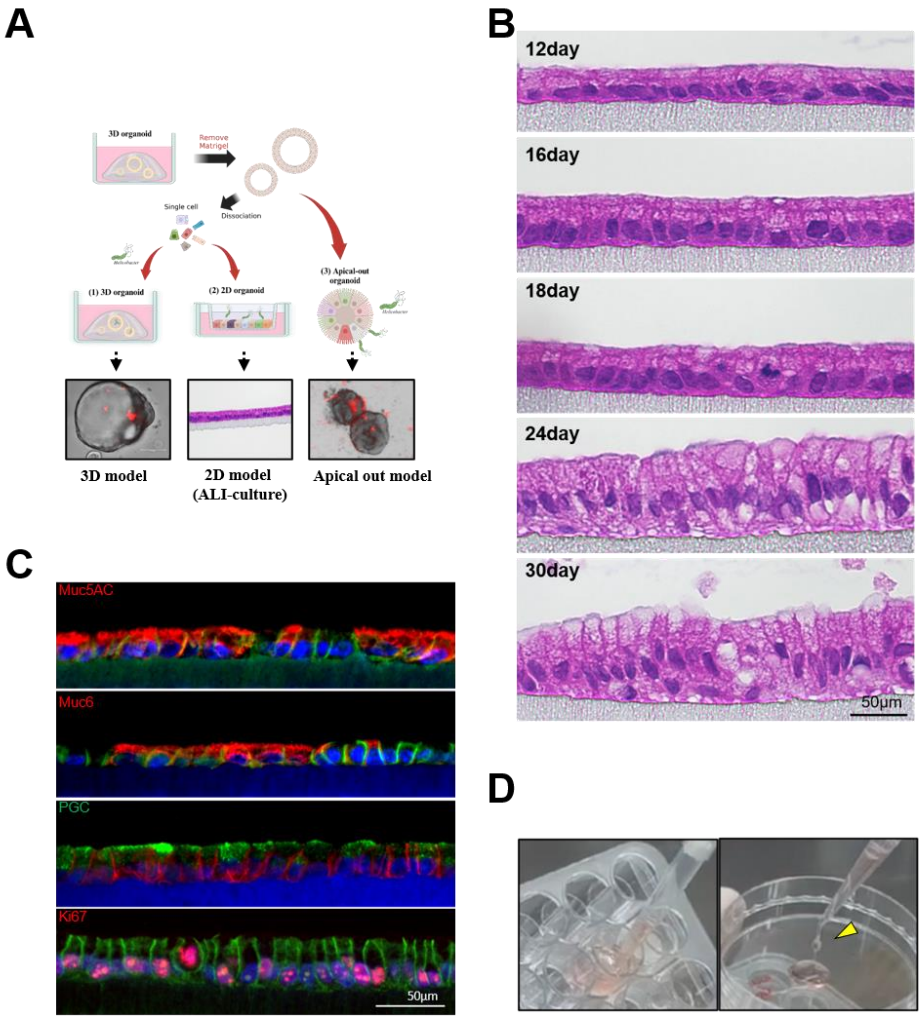

Supplementary Figure 7. *H. pylori* infection model in human gastric 2D organoids (mucosoid). (A) Three systems for *H. pylori* infection in human gastric organoids: *H. pylori* infection via physical disruption of organoids, conversion to 2D organoids (mucosoid), and induction of the apical-out model. (B) H&E images showing an increase in height and polarization of the cell layer. Scale bar: 50 μm. (C) Immunofluorescence staining analysis revealed MUC5AC and MUC6 granules, with PGC-positive cells detected on the apical side of the 2D organoids. (D) Under air-liquid interface conditions, 2D organoids (mucosoid) produce mucus within the monolayer (day 10 of culture).

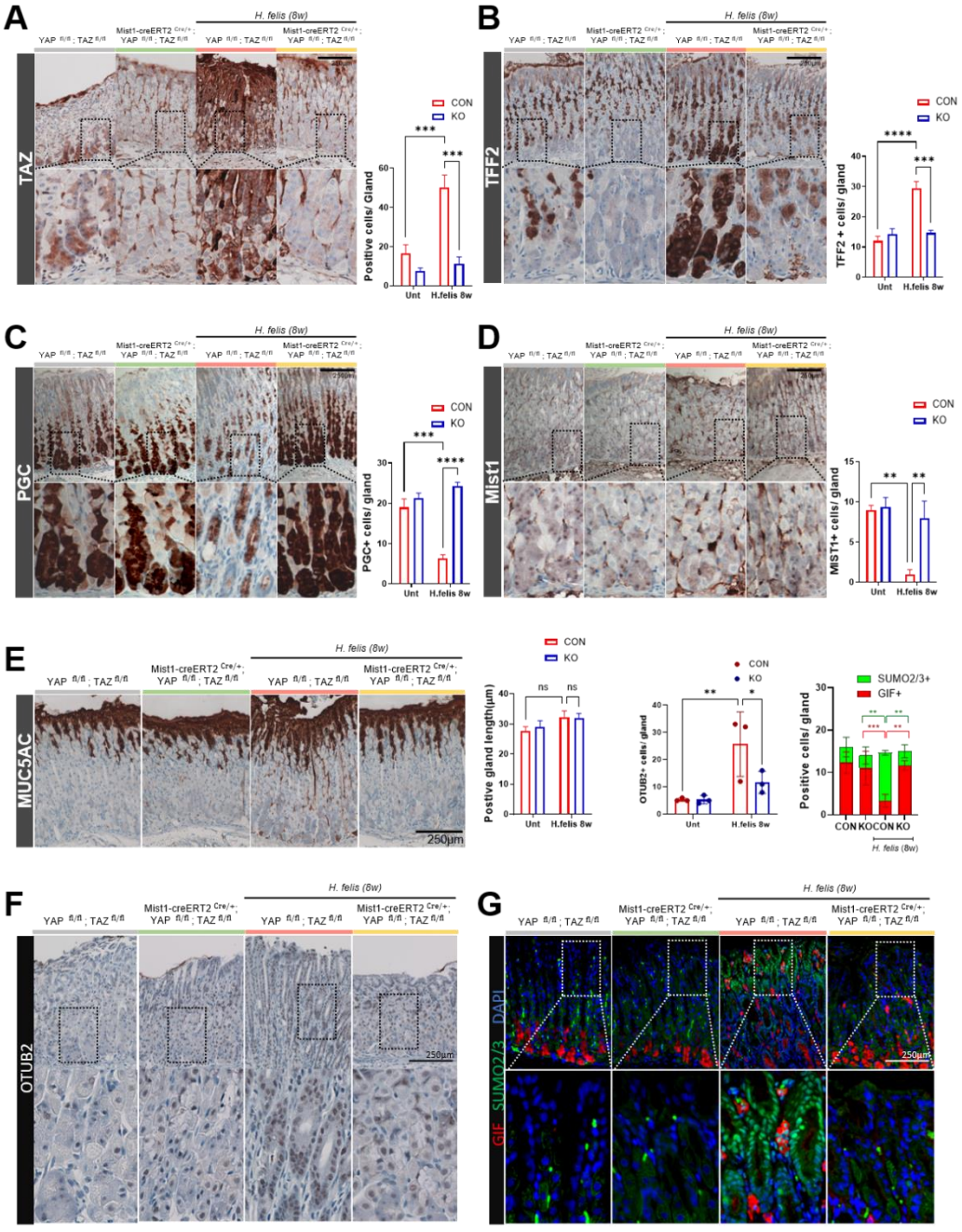

Supplementary Figure 8. Histopathological analysis of YAP / TAZ $^{fl/fl}$ and Mist1-creERT2 $^{Cre/+}$; YAP / TAZ $^{fl/fl}$ mice infected with *H. felis.* Representative

immunohistochemical staining images for (A) TAZ, (B) TFF2, (C) PGC, (D) Mist1, (E) Muc5AC, and (F) OTUB2 in the stomach of each group of mice. Scale bar: 250 μm. Each graph represents the number of positive cells from a single gland (n = 3 per group). (G) Representative immunofluorescence staining images for SUMO2/3 and GIF from the stomach of mice in each group (n = 3 per group). Scale bar: 250 μm. Statistical analysis was performed using two-way analysis of variance with Tukey's multiple comparisons : *P < 0.05; **P < 0.01; ***P < 0.001 ; ****P < 0.0001. All data are presented as means ± SEM.

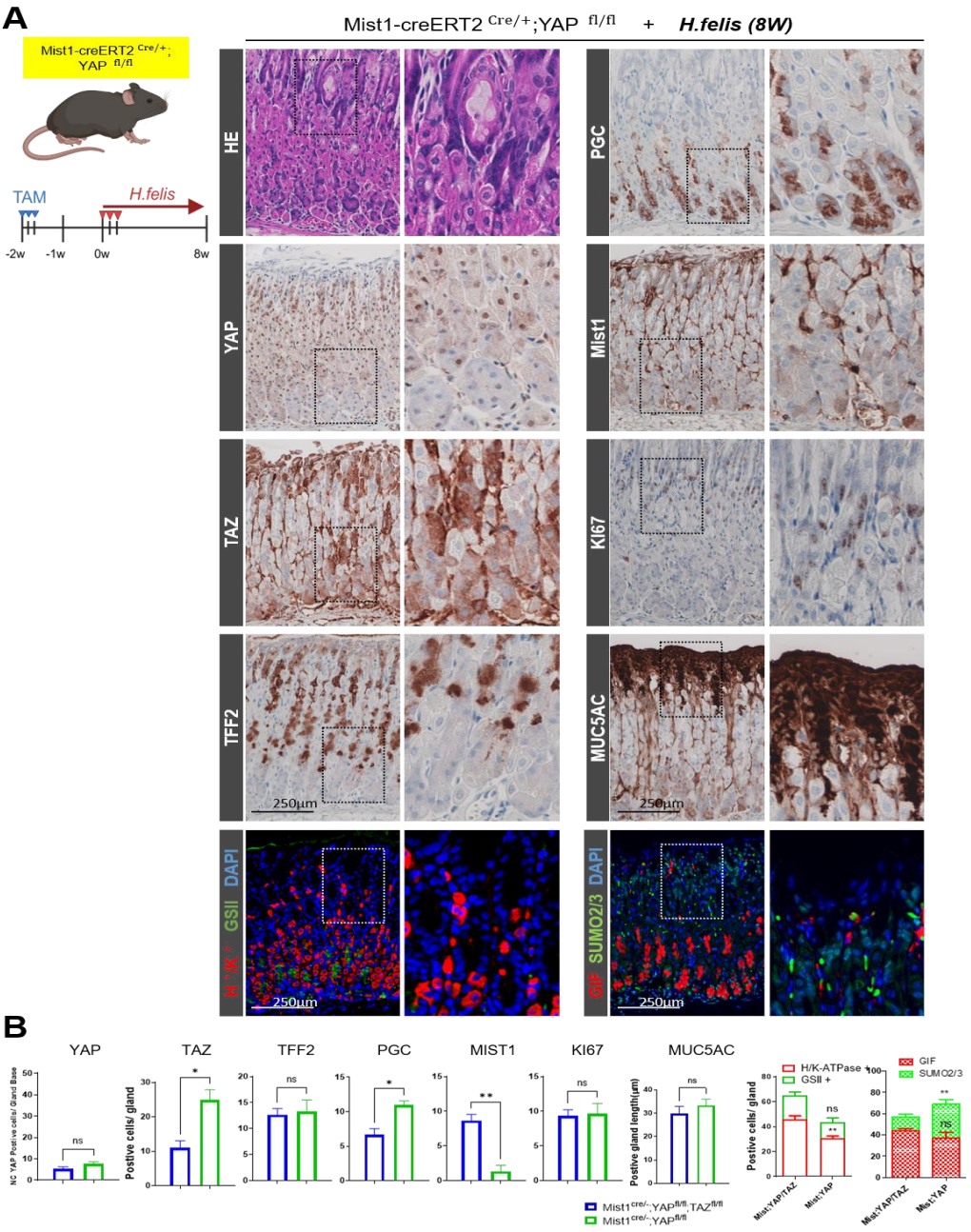

Supplementary Figure 9. Histopathological analysis of Mist1-creERT2 $^{Cre/+}$; YAP $^{fl/fl}$ mice single knockout mice infected with *H. felis*. (A) Representative immunohistochemical staining

images for HE, YAP, TAZ, TFF2, PGC, Mist1, Ki67, MUC5AC in the stomachs of YAP KO mice. Representative fluorescent staining images for H^+/K^+-ATPase, GSII, GIF, SUMO2/3 in the stomach of YAP KO mice. Scale bar: 250 μm. (B) Comparison of positive cells in YAP/TAZ double-knockout mice and YAP single-knockout mice infected with *H. felis.* Each graph represents the number of positive cells in a single sample (n = 3 per group). Statistical analysis was performed using two-way analysis of variance with Tukey's multiple comparisons and two-tailed unpaired Student's t-test: *P < 0.05; **P < 0.01; ***P < 0.001. All data are presented as mean ± SEM.

Supplementary material 1. Antibodies and Primers

The following primary antibodies and primers were purchased commercially or kindly provided by colleagues and were used for immunohistochemistry, Western blot, and immunofluorescence analyses:

Antibodies	**Source**	**Cat. No.**	
YAP	Cell signaling	4912S	YAP Antibody
TAZ	BD	560235	Purified Mouse anti-TAZ Clone M2-616(RUO)
YAP/TAZ	Cell signaling	8418S	YAP/TAZ(D24E4) Antibody
LATS2	Cell signaling	5888S	LATS2(D83D6) antibody
CDX2	Abcam	ab76541	Anti-CDX2 antibody(EPR2764Y)
TFF2	invitrogen	PA5-57781	TFF2 Polyclonal antibody
MUC5AC	Abcam	ab77576	Anti-Mucin 5AC antibody(CLH2)
MUC6	Abcam	ab212646	Anti-Gastric Mucin antibody(CLH5)
Mist1	Santa Cruz	sc-80984	MIST1 antibody(6E8)
PGC	Novus Biologicals	NBP1-91011	Pepsinogen C/PGC/Progastricsin antibody
CagA	Santa Cruz	sc-28368	CagA-Antibody
MST1/2	invitrogen	PA5-36100	MST1/MST2 Polyclonal antibody
ZO-1	invitrogen	339100	MOUSE ANTI ZO-1(ZO1-1A12)
CD44v9	CosmoBio	CAC-LKG-M00	Anti CD44 Antigen v10-e16 mAb (Clone RM1)
Snail	Cell signaling	3879s	Snail(C15D3) Rabbit mAb
TEAD1	Cell signaling	12292S	TEAD1(D9X2L) Rabbit mAb
E-cadherin	abcam	ab407732	Anti-E cadherin antibody(EP700Y)
OTUB2	ATLAS	HPA002329	Anti-OTUB2

OTUB2	invitrogen	PA5-99680	OTUB2 Polyclonal Antibody
YAP1	Abnova	H00010413-M01	YAP1 monoclonal antibody (M01), clone 2F12 [100 ug]
P-YAP	Cell signaling	4911	Phospho-YAP (Ser127) Antibody #4911
Lamin B	Santa Cruz	sc-374015	Lamin B1 Antibody (B-10)
SUMO2/3	Cell signaling	4971	SUMO-2/3 (18H8) Rabbit mAb #4971

Primers for Mouse Genotyping		
Mist-cre	Mist1-creERT(1)	ggtttaagcaaattgtcaagtacgg (25 mer)
	Mist1-creERT(2)	atagtaagtatggtggcggtcagcg (25 mer)
	Mcre-CER	gaagcattttccaggtatgctcag (24 mer)
TAZ-flox	Wwtr1 (F) Mut 400_ WT 314	CTTCCAAGGTGCTTCAGAGA (20 mer)
	Wwtr1 (R) Mut 400_ WT 314	GGAGAGGTAAAGCCCACCAG (20 mer)
YAP-flox	Yap1 (F) Mu 400 WT 300	GTCTTTCTCTAGGCACAAAAAGG (23 mer)
	Yap1 (R) Mu 400 WT 300	AGTGGTAAAGAATAATGCTCATCC (24 mer)

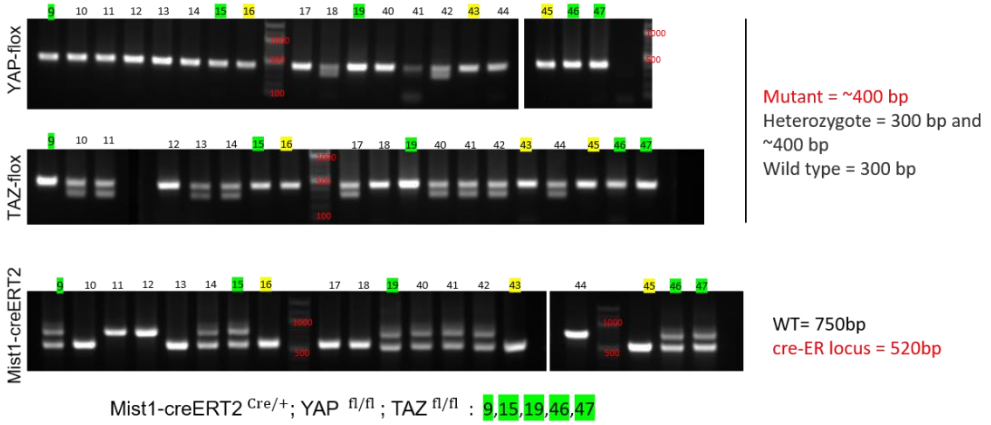

Genotyping of mouse strains. DNA was isolated from mouse tails, and PCR products were generated with primer sequences as described in the "Supplementary Material 1" PCR of the YAP/TAZ fluxed gene generated 400 bp. The cre-ER locus (mutant) of Mist1-CreERT2 generated 520 bp

Primers for Real time PCR	
OTUB2 (F)_375bp	CCTGCTTTTGACTGGGTTCC (20 mer)
OTUB2 (R)_375bp	CTCATGGTTCCCCTGACACT (20 mer)
YAP1(F)_783bp_22.07.27	AGGGAGGAAGGAAGGAACAA (20 mer)
YAP1(R)_783bp_22.07.27	GAGAAACAGCTCCCAACTGC (20 mer)
YAP1(F)_1911bp_22.07.27	GCAGTTGGGAGCTGTTTCTC (20 mer)
YAP1(R)_1911bp_22.07.27	CCTAGGTTCCGACAAAACCA (20 mer)
CDX2 (F) _20.10.27	GACGTGAGCATGTACCCTAGC (21 mer)
CDX2 (R)_20.10.27	GCGTAGCCATTCCAGTCCT (19 mer)
MUC2(F) -20.10.27	ACAACTACTCCTCTACCTCCA (21 mer)
MUC2(R) -20.10.27	GTTGATCTCGTAGTTGAGGCA (21 mer)
GAPDH (F) _332bp_22.07.27	CGACCACTTTGTCAAGCTCA (20 mer)
GAPDH (R) _332bp_22.07.27	AGGGGTCTACATGGCAACTG (20 mer)
ZO-1 (F)	AGAAGATAGCCCTGCAGC (18 mer)
ZO-1 (R)	AGTCCATAGGGAGATTCC (18 mer)
Snail (F)	CCCCAATCGGAAGCCTAACT (20 mer)
Snail (R)	GGTCGTAGGGCTGCTGGAA (19 mer)
IL-8_(F)	ACACTGCGCCAACACAGAAAT (21 mer)
IL-8_(R)	ATTGCATCTGGCAACCCTACA (21 mer)
CTGF_(F)	GGAAAAGATTCCCACCCAAT (20 mer)
CTGF_(R)	TGCTCCTAAAGCCACACCTT (20 mer)

Abstract in Korean

YAP/TAZ 신호조절을 통한 헬리코박터 매개 위암 발병 및 진행 제어

헬리코박터 파일로리(*H. pylori*)는 상피세포에서 만성염증성신호전달 경로를 활성화하여 위암 위험을 증가시키는 것으로 알려져 있으며, 헬리코박터 파일로리 세포독소 관련 단백질 A (CagA)는 인간 위암 발병에 중요한 역할을 하는 것으로 알려져 있다. 히포 신호전달의 구성 요소인 YAP/TAZ의 과발현과 신호 조절 장애는 종양을 유도하고, 세포 증식과 세포 사멸 저항성을 촉진하는 것으로 보고되었다. 그러나 헬리코박터 매개 위암 발생에서 YAP/TAZ의 역할은 아직 완전히 규명되지 않았다. 이번 연구에서 인간 위 조직의 싱글셀 분석과 공개된 TCGA 데이터를 통해 YAP이 위암 발생에서 중요하게 작용됨을 확인했다. YAP 과발현은 장상피화생 표지자인 CDX2 발현을 유도하고 결합 단백질 ZO-1을 하향 조절하여 세포 이동성을 증가시킨다. 탈유비퀴틴화 효소인 OTUB2는 YAP의 분해를 방지하여 핵 전좌와 위암 관련 유전자 표현을 촉진한다. 또한 헬리코박터 매개 위암 발병 단계에서 주세포의 전환분화에 YAP/TAZ가 기여할 가능성을 확인하기 위해 타목시펜/Cre-loxP 시스템을 사용하여 Mist1-creERT2 $^{Cre/+}$; YAP / TAZ $^{fl/fl}$ 마우스를 제작했다. *H. pylori*보다 마우스에서 재현성이 높은 *H. felis* 감염 마우스 모델을 이용하여 인간 조직 변화와 유사한 병변을 유도하고 위 전암성 장상피화생의 발달에서 YAP/TAZ의 역할을 규명했다. 또한 야생형 마우스에 외인성 재조합 OTUB2와 OTUB2 억제제를 투여하여 위선 세포의 화생성 변화에 미치는 영향을 조사하고 잠재적인 조절 메커니즘을 식별했다. 결론적으로 헬리코박터 매개 위암 발병 및 진행에서 YAP/TAZ 신호조절은 중추적인 역할을 하며, OTUB2가 YAP 활성화의 고유 조절자 역할을 하고 있음을 확인했다. 이러한 발견은 헬리코박터 매개 위암 발생 및 진행에서 YAP/TAZ 신호 조절을 통한 암 제어 가능성의 학문적 기반을 제공한다.

핵심되는 말 : 위암, 상피화생, 헬리코박터, YAP, OTUB2, CagA